NASA Technical Memorandum 85795

Low-Speed Investigation of Effects of Wing Leading- and Trailing-Edge Flap Deflections and Canard Incidence on a Fighter Configuration Equipped With a Forward-Swept Wing

Thomas G. Gainer, Michael J. Mann,
and Jarrett K. Huffman

JULY 1984

NASA

NASA Technical Memorandum 85795

Low-Speed Investigation of Effects of Wing Leading- and Trailing-Edge Flap Deflections and Canard Incidence on a Fighter Configuration Equipped With a Forward-Swept Wing

Thomas G. Gainer, Michael J. Mann,
and Jarrett K. Huffman
Langley Research Center
Hampton, Virginia

NASA

National Aeronautics
and Space Administration

**Scientific and Technical
Information Branch**

1984

SUMMARY

An investigation has been made in the Langley 7- by 10-Foot High-Speed Tunnel to study the effects of wing leading- and trailing-edge flap deflections and canard incidence on the longitudinal aerodynamic characteristics of an advanced fighter configuration with forward-swept wing. The wing had 29.5° forward sweep of the quarter-chord line and an aspect ratio of 3.28. The leading- and trailing-edge flaps had chords of 15 percent and 30 percent of the wing chord, respectively, and extended to the 0.839 spanwise station. The canard had an aspect ratio of 3.28 and 45° of rearward leading-edge sweep. The effects of strakes added to the fuselage ahead of the wing were also investigated with and without the canard. Tests were made at a Mach number of 0.3 through a range of angle of attack from about -2° to 22°.

The test results showed that deflecting the flaps significantly improved the lift-drag characteristics at the higher angles of attack. The canard was able to trim the configurations with different flap deflections over most of the range of angle of attack. The penalty in maximum lift coefficient due to trimming was about 0.10.

INTRODUCTION

The present investigation was made to expand the existing data base for forward-swept wings by providing data on the effects of leading- and trailing-edge flap deflections on the longitudinal characteristics at low speed of an advanced forward-swept wing fighter design. The configuration tested had a close coupled canard for longitudinal control and was designed to be highly maneuverable at both subsonic and transonic speeds.

Forward-swept wings have received a good deal of attention now that it appears that the aeroelastic divergence problem associated with forward sweep can be overcome by the use of composite wing structures. (See ref. 1.) A forward-swept wing would have several advantages. Because the air tends to flow toward the root rather than toward the tip as it does on a sweptback wing, the flow on a forward-swept wing tends to separate first at the inboard sections while good flow conditions can be maintained at the tip. These conditions result in improved stall characteristics and allow the ailerons to remain effective at high angles of attack, even after the main part of the wing has stalled. By placing a canard or other aerodynamic surface ahead of the wing, favorable interference could be provided over the inboard portion of the wing where the shock is strongest (and shock-induced separation the greatest) at high subsonic and transonic speeds. This favorable interference would significantly improve maneuvering performance.

Other advantages of the forward-swept wing arise from the more favorable weight and area distributions that result from having the wing root located at the rear of the fuselage rather than at midlength as it is for sweptback wings. When area ruling is applied to a forward-swept wing configuration, the fuselage is made narrow toward the rear while a larger fuselage volume can be maintained forward at the center-of-gravity location; this allows fuel to be stored at the center of gravity without the usual center-of-gravity shifts that occur as the fuel is used. The forward-swept wing arrangement also places the ailerons longitudinally closer to the center of

gravity so that there is very little change in pitching moment when ailerons are used for roll control.

Forward-swept wings have been investigated in a number of studies; references 2 through 4, for example, describe the results of detailed design studies that included investigations of the effects of trailing-edge flaps. More information is needed, however, particularly on leading-edge flaps used in conjunction with trailing-edge flaps, in order to evaluate and design flap arrangements for forward-swept wings.

In the present investigation, low-speed tests were made in the Langley 7- by 10-Foot High-Speed Tunnel on a model with a forward-swept wing of aspect ratio 3.28 with close coupled canard. The wing was equipped with a 15-percent-chord leading-edge flap and a 30-percent-chord trailing-edge flap which could be deflected up to 20°. Trimming effects were determined for some configurations by testing through a range of canard incidence from +10° to -20°. The effects of a forebody strake were also investigated, with and without the canard in place. The tests were made at a Mach number of 0.3. Static longitudinal forces and moments were measured through a range of angle of attack from about -2° to 22° at 0° sideslip.

SYMBOLS

Force and moment coefficients are based on the geometry of the basic trapezoidal wing extended to the model centerline. (See table I.) Pitching moments are referred to a moment center at 60.71 cm (23.9 in.) from the fuselage nose (15.6 percent of the mean aerodynamic chord). Dimensions are given in both SI and U.S. Customary Units.

b wing span, 67.686 cm (26.648 in.)

$\bar{c}$ wing mean aerodynamic chord, 23.518 cm (9.259 in.)

C_D drag coefficient, $\frac{\text{Drag}}{qS}$

C_L lift coefficient, $\frac{\text{Lift}}{qS}$

$C_{L,max}$ maximum lift coefficient

C_m pitching-moment coefficient, $\frac{\text{Pitching moment}}{qS\bar{c}}$

C_N normal-force coefficient, $\frac{\text{Normal force}}{qS}$

i_c canard incidence, positive with canard trailing edge down, deg

L/D lift-drag ratio

q free-stream dynamic pressure, Pa (lb/ft^2)

S wing area, 0.139 m^2 (1.50 ft^2)

x_{mr} distance from model nose to moment reference center, measured parallel to model centerline, cm (in.)

$\bar{x}$ distance from model nose to trim point, measured parallel to model center line, cm (in.)

α angle of attack, deg

δ_{le} leading-edge flap deflection, positive with flap leading edge down, deg

δ_{te} trailing-edge flap deflection, positive with flap trailing edge down, deg

FRP fuselage reference plane

η spanwise station, nondimensionalized with respect to b/2

MODEL DESCRIPTION

The general arrangement of the model and drawings of the wing sections, fuselage cross sections, and fuselage strakes are shown in figure 1. Photographs of the model installed in the 7- by 10-Foot High-Speed Tunnel are shown in figure 2. A detailed listing of the geometric characteristics of the model is given in table I.

The configuration was designed for good transonic maneuver performance by use of the transonic wing canard fuselage code of reference 5. The design featured close coupling of the wing and canard and careful cambering and twisting of the wing sections to provide large regions of supercritical flow and a minimum of shock-induced separation at transonic speeds. The general shapes of the wing sections are shown in figure 1(b). Each section was 4.44-percent thick and had a nose radius equal to 0.54 percent of the local wing chord. The wing twist distribution is shown in figure 3. The wing had -2° incidence at the fuselage juncture; the twist then increased in two linear segments between the fuselage juncture and $\eta = 0.9$ and was a constant 4° outboard of $\eta = 0.9$.

The leading- and trailing-edge flaps extended from the fuselage juncture to the station at $\eta = 0.839$. (The photographs of fig. 2 show that the flaps were segmented, but all segments were deflected uniformly and the flaps were treated as integral units, as shown in fig. 1.) The leading-edge flap chord was 15 percent of the local wing chord; the trailing-edge flap chord was 30 percent of the local chord. As shown in figure 1(b), brackets were used to set the flap deflections, with body fill used in the crevices formed by deflecting the flaps. Deflections of 0°, 5°, 10°, and 20° were investigated for both the leading- and trailing-edge flaps.

The canard, which was located ahead of and above the wing, was pivoted about the hinge line shown in figure 1(a). It had the same aspect ratio as the wing (3.28) but 45° of rearward leading-edge sweep instead of forward sweep. The exposed canard area was 15.6 percent of the wing reference area. The canard had 10° dihedral and the twist distribution shown in figure 3. Canard incidences from +10° to -20°, in 5° increments, were investigated.

The model was area-ruled by using the method of references 6 through 9 to reduce the zero-lift wave drag for Mach numbers between 1.0 and 1.6. The fuselage cross sections (fig. 1(c)) were circular fore and aft of the canopy region. The sides of

the fuselage were made flat in the region of the canard to keep the canard flush with the fuselage as it went through a range of incidence angle.

The model was also tested with the fuselage strakes shown in figure 1(d). These strakes were designed with the use of the criterion and theoretical methods of reference 10. The strakes were mounted below the wing reference plane and blended in with the wing leading edge as shown. Strake tests were made both with the canard on and off.

APPARATUS AND TESTS

The tests were made in the Langley 7- by 10-Foot High-Speed Tunnel with the test section in the solid wall configuration. This is a continuous-flow, single-return atmospheric tunnel with rectangular test section. A description of the tunnel is given in reference 11.

Aerodynamic forces and moments were measured with an internally mounted, six-component strain-gauge balance. The angle of attack of the model was measured with a pendulous inertial accelerometer mounted in the model nose. Static pressures for use in drag corrections were measured at the model base and in the balance cavity.

The tests were made through a range of angle of attack from about -2° to 22° at 0° sideslip. All tests were made at a Mach number of 0.3, which corresponded to a dynamic pressure of about 10 kPa (125 lb/ft^2) and a Reynolds number based on the wing mean aerodynamic chord of $4.82 \times 10^6/m$ ($1.47 \times 10^6/ft$).

CORRECTIONS

Transition strips about 0.159 cm (0.063 in.) wide of No. 90 carborundum grains were placed 2.54 cm (1.0 in.) aft (streamwise) of the leading edge on the wing, canard, vertical tail, and strakes. A strip of the same width but of No. 100 carborundum grains was placed 2.54 cm (1.0 in.) aft of the fuselage nose.

The model angle of attack was corrected for tunnel flow angularity. Jet boundary and blockage corrections, based on the procedures of references 12 and 13, respectively, were applied to the data. Drag measurements were adjusted to the condition of free-stream pressure acting over the model base.

PRESENTATION OF DATA

In addition to the graphical presentation of data in this report, the wind-tunnel data are available in machine-readable form. A complete set of body and stability axis coefficient data is available on an electronic publication standard interface format tape from

National Technical Information Service (NTIS)
5285 Port Royal Road
Springfield, VA 22161

Requestors should ask for Data Tape Supplement to NASA TM-85795.

RESULTS AND DISCUSSION

Lift-Drag Characteristics

Basic data showing the effects of canard and canard incidence for the different wing trailing-edge flap deflections investigated are shown in figure 4. (Note, the leading-edge flap deflection for these tests was 10° for all cases except $\delta_{te} = 0°$ where it was 0°.) Comparing the data for canard on with those for canard off shows that the canard provided a substantial amount of lift at the higher angles of attack, even at the negative canard incidence required for trim. Adding the canard increased both the lift-curve slope and the angle of attack for $C_{L,max}$. Analysis of data obtained with the canard and fuselage, the wing and fuselage, and the fuselage alone indicates that the lift improvements are equivalent to the lift of the canard by itself with very little incremental lift due to mutual interference effects.

The variations in lift coefficient with canard incidence for angles of attack up to that for $C_{L,max}$ are shown in figure 5, for the flaps undeflected and flaps-deflected case. These variations were linear at the lower angles of attack and negative canard incidences but then leveled off because of canard stall at the higher angles of attack and positive canard incidences. The data indicate that the leveling off occurred when the geometric angle of attack of the canard ($i_c + \alpha$) reached about 18° (represented by the dashed lines in fig. 5). The configuration with $i_c = 0°$ generally gave the highest lift at the higher angles of attack for all trailing-edge deflections. Positive canard incidences were not effective in producing lift at the higher angles of attack.

The lift-drag data of figure 4 show that, in the higher lift coefficient range, adding the canard reduced the drag and increased L/D at a given lift coefficient. This result was to be expected because at these higher lift coefficients, the wing was developing very little leading-edge suction, so that the resultant force on the wing was almost normal to the wing chord plane. When this is true, L/D is mainly a function of the angle of attack, and the higher lift-drag ratios at a given lift coefficient with canard on were the result of the configuration being at a lower angle of attack than with the canard off.

The effects of wing trailing-edge flap deflection, for $i_c = 0°$ and $\delta_{le} = 0°$, are shown in figure 6. As might be expected, deflecting the trailing-edge flap shifted the curve of lift against angle of attack toward a more positive lift without changing the lift-curve slope. Deflecting the trailing-edge flap also reduced the angle of attack for $C_{L,max}$, indicating some flow separation was present with the trailing-edge flap deflected. The lift effectiveness of the trailing-edge flap was about 0.024 per degree at the lower flap deflections and about 0.013 per degree at the higher flap deflections.

The data in figure 6(b) show that each deflection of the trailing-edge flap provided improvement in the lift-drag characteristics at some point in the range of lift coefficient; that is, deflecting the flap 5° provided small increases in L/D in the lift coefficient range between about 0.55 and 0.90; deflecting the flap 10° provided further small increases in the lift coefficient range between about 0.9 and 1.2. However, most of the improvements were confined to lift coefficients above 1.2, where there were large reductions in drag and increases in L/D at a given lift coefficient as the trailing-edge flap deflection was increased. For example, at a lift coefficient of 1.35, which was the maximum lift coefficient with flaps undeflected, the drag was reduced by almost 50 percent by deflecting the trailing-edge flap from 0° to 20°. At $C_L = 1.35$, deflecting the flap 20° increased L/D from

about 2.5 to about 5.0. At $C_{L,max}$, L/D was increased by a smaller but still substantial amount - from about 2.5 to about 3.5; this value of L/D of 3.5, of course, occurred at a much higher $C_{L,max}$ than with the flap undeflected.

The effects of leading-edge flap deflection for each of the trailing-edge flap deflections in figure 6 are shown in figure 7. Deflecting the leading-edge flap increased the lift-curve slope but reduced the lift over most of the lower range of angle of attack. The main advantage of deflecting the leading-edge flap was that it extended the lift curves to a much higher $C_{L,max}$, indicating that leading-edge flap deflection eliminated at least some of the flow separation caused by deflecting the trailing-edge flap. At the higher angles of attack, the increments in lift provided by leading-edge flap deflection were equally as large as those provided by trailing-edge flap deflection. The effects of both leading- and trailing-edge flap deflection on $C_{L,max}$ are shown in figure 8. These data show that a given increment in $C_{L,max}$ could be produced by deflecting either the trailing-edge or the leading-edge flap through a given angle and that these increments were additive. For example, deflecting either the leading- or the trailing-edge flap 20° increased $C_{L,max}$ by about 0.2. Deflecting both flaps 20° produced an increase in $C_{L,max}$ of 0.4.

Unlike deflecting the trailing-edge flap, deflecting the leading-edge flap improved the lift-drag characteristics only at the higher lift coefficients. In the lower range of lift coefficient, deflecting the leading-edge flap through a large angle substantially reduced L/D. (The one exception was the data for $\delta_{le} = 10°$ and $\delta_{te} = 10°$ in fig. 7(c), which show that the leading-edge flap deflection of 10° produced a proportionately higher L/D over most of the range of lift coefficient.) As with the trailing-edge flap, deflecting the leading-edge flap produced only a small improvement in the L/D at $C_{L,max}$; however, it allowed a lift-drag ratio of between about 2.5 and 3.5 to be maintained at a much higher $C_{L,max}$.

The effects of the strakes on the longitudinal aerodynamic characteristics are shown in figure 9, which compares data for the four different wing, strake, and canard combinations tested. These data show that the strakes were as effective as the canard in providing lift throughout most of the range of angle of attack, but then more effective at angles above about 20°. The lift-curve slope for the wing-plus-strakes configuration showed a sharp increase above $\alpha = 20°$, whereas that for the wing-plus-canard configuration showed a leveling off at these angles. The configuration with both strakes and canard gave much higher lift than either the wing-plus-strakes or the wing-plus-canard configuration, especially at the higher angles of attack. The increased lift obtained by adding the strakes along with the canard was about the same as that which could be obtained with a trailing-edge flap deflection of 10° more. That is, the wing-plus-canard-plus-strakes configuration with $\delta_{le} = 10°$ and $\delta_{te} = 10°$ gave about the same or higher lift at the higher angles of attack as the wing-plus-canard configuration with $\delta_{le} = 10°$ and $\delta_{te} = 20°$. (See fig. 4(d).)

The wing-plus-strakes configuration gave much lower values of L/D than the wing-plus-canard configuration over most of the range of lift coefficient. The L/D characteristics of the wing-plus-canard-plus-strakes configuration were about the same as those for the wing-plus-strakes configuration at the lower lift coefficients and were about the same as those for the wing-plus-canard configuration at the higher lift coefficients.

The effects of canard incidence on the longitudinal aerodynamic characteristics of the wing-plus-canard-plus-strakes configuration are shown in figure 10. These data show the same loss in canard effectiveness for 10° canard incidence at the

higher angles of attack that occurred for the wing-plus-canard configuration (fig. 4(c)), but also show that smaller lift decrements were produced by negative canard incidences than with the canard alone.

The lift increments produced by deflecting the trailing-edge flap for the wing-plus-strake configuration (fig. 11) were about the same as those for the wing-plus-canard configuration (fig. 6).

Pitching-Moment Characteristics

The moment reference center about which the data are presented was one about which the different configurations could be trimmed over most of the range of angle of attack. To determine this reference center, the locations of trim points $\bar{x}$, that is, the points about which the pitching moment would be zero, were calculated from the equation:

$$\frac{\bar{x}}{\bar{c}} = \frac{x_{mr}}{\bar{c}} - \frac{C_m}{C_N}$$

and then analyzed to determine the most suitable location. The results of these calculations are shown in figure 12 as a function of trim angle of attack for different canard incidences. The data are shown for the two extreme cases for which canard effectiveness data were obtained: the case with flaps undeflected and the case with the leading-edge flap deflected 10° and the trailing-edge flap deflected 20°.

The data show that to trim at the higher angles of attack, the moment reference center would have to be located in the fairly narrow region between about $\bar{x}$ = 59.4 cm (23.4 in.) and $\bar{x}$ = 61.5 cm (24.2 in.). For a moment reference center any farther forward than this, the canard would not develop enough positive normal force to trim out the negative pitching moment developed by the wing; for a moment reference center farther aft than this region, the canard would not develop enough negative normal force, at least at -20° deflection, to balance out the wing moment. The data at the higher angles of attack show the effects of canard stall; that is, no more positive lift could be developed by going from 0° to 5° or 10° canard incidence. Hence, the moment reference center for trim could not be moved any farther forward by using positive canard deflections.

With the moment reference center within the range between 59.4 cm (23.4 in.) and 61.5 cm (24.2 in.), the configuration with δ_{le} = 0° and δ_{te} = 0° could be trimmed at 0° angle of attack; the configuration with δ_{le} = 10° and δ_{te} = 20° could not be trimmed, at least for a canard incidence as high as 10°. But since there was no evidence of canard stall for i_c = 10° at α = 0°, the configuration with flaps deflected could also probably be trimmed at 0° angle of attack by going to a canard incidence higher than 10°.

The moment reference center selected for presenting the data in this report was x_{mr} = 60.7 cm (23.9 in.); this location allowed the configuration with flaps deflected to be trimmed from α = 4° to about 22°.

For the moment reference center selected, the model was about neutrally stable with canard off. (For example, see fig. 4(a).) Adding the canard made it unstable,

with the instability tending to be greater at the higher angles of attack. With the canard on, the value of $\partial C_m/\partial C_L$ was about 0.2 (an unstable static margin) at the lower angles of attack and about 0.3 at the higher angles of attack before stall.

Deflecting the trailing-edge flap had no significant effect on the static longitudinal stability, but deflecting the leading-edge flap tended to reduce the canard-on instability at both the lower and the higher angles of attack. For example, for a fixed trailing-edge deflection, increasing the leading-edge deflection from 0° to 20° decreased $\partial C_m/\partial C_L$ from about 0.3 to about 0.2. The data indicate that, because of this decrease, the level of unstable values of $\partial C_m/\partial C_L$ could be kept below about 0.23 over most of the range of angle of attack by using a deflection schedule for the leading-edge flap. The configuration could have this static margin at the lower angles of attack with the flaps undeflected and at the higher lift coefficients with the flaps deflected.

Trimmed lift-drag ratios are shown in figure 13 for the four configurations for which canard effectiveness data were obtained. The penalty in $C_{L,max}$ that resulted from trimming amounted to about 0.1 at all trailing-edge flap deflections. For each configuration, there was no trim drag penalty over a certain range of lift coefficient. For example, for the configurations with $\delta_{le} = 0°$ and $\delta_{te} = 0°$, the trimmed L/D and untrimmed L/D were about the same for a range of lift coefficient from about 0.7 to about 0.9. This range shifted to higher lift coefficients as the trailing-edge flap deflection was increased.

The strakes had a destabilizing effect on the pitching moments (fig. 9). The wing-plus-canard-plus-strakes configuration in particular had a higher level of longitudinal instability than the wing-plus-canard configuration throughout the range of angle of attack. Because adding the strakes caused the canard to lose some effectiveness in changing the lift at negative deflections, the wing-plus-canard-plus-strakes configuration with $\delta_{le} = 10°$ and $\delta_{te} = 10°$ could be trimmed to an angle of attack of only about 12°, which corresponds to a lift coefficient of about 1.2. This value was well below $C_{L,max}$ of about 1.5 to which the wing-plus-canard configuration could be trimmed.

CONCLUSIONS

Tests in the Langley 7- by 10-Foot High-Speed Tunnel at low speed (Mach 0.3) of a forward-swept wing fighter configuration with canard and deflectable wing leading- and trailing-edge flaps indicated the following conclusions:

1. Deflecting the leading- and trailing-edge flaps, either separately or in combination, significantly improved the high-angle-of-attack performance of the forward-swept wing configuration.

2. The canard contributed a substantial amount of the lift at the high angles of attack. At the higher lift coefficients, adding the canard also reduced the drag and increased the lift-drag ratio at a given lift coefficient. The canard showed signs of stalling when the combination of canard incidence plus wing angle of attack reached about 18°.

3. The increments in maximum lift coefficient produced by deflecting either the leading- or the trailing-edge flap were about the same. Deflecting the trailing-edge flap shifted the lift curve in the positive direction without changing the lift-curve

slope; deflecting the leading-edge flap then extended the lift curve to a higher angle of attack for stall without a significant change in lift-curve slope.

4. The configuration with both strakes and canard gave much higher lift than either the wing-plus-strakes or the wing-plus-canard configuration, especially at the higher angles of attack. At the higher angles of attack, lift-drag ratios for the wing-plus-canard-plus-strakes configuration were about the same as those for the wing-plus-canard configuration.

5. A narrow range of moment reference centers was found for which the different configurations could be trimmed over most of the range of angle of attack. For the moment reference center chosen, the model was about neutrally stable with canard off; adding the canard made it unstable, with the instability tending to be greater at the higher angles of attack. Deflecting the leading-edge flap had a stabilizing effect at the higher angles of attack.

6. The penalty in maximum lift coefficient that resulted from longitudinal trimming amounted to about 0.1 for all trailing-edge flap deflections.

Langley Research Center
National Aeronautics and Space Administration
Hampton, VA 23665
June 5, 1984

REFERENCES

1. Krone, Norris J., Jr.: Divergence Elimination With Advanced Composites. AIAA Paper No. 75-1009, Aug. 1975.

2. Miller, B. D.; and Hadley, S. K.: Application of Forward Swept Wings to an Air Combat Fighter. AIAA-83-1833, July 1983.

3. Moore, M.; and Frei, D.: X-29 Forward Swept Wing Aerodynamic Overview. AIAA-83-1834, July 1983.

4. Grafton, Sue B.; Gilbert, William P.; Croom, Mark A.; and Murri, Daniel G.: High Angle-of-Attack Characteristics of a Forward-Swept Wing Fighter Configuration. AIAA-82-1322, Aug. 1982.

5. Aidala, P.: Numerical Aircraft Design Using 3-D Transonic Analysis With Optimization. Volume III. Part 2: User's Guide to Fighter Design Computer Program. AFWAL-TR-81-3091, Vol. III, Pt. 2, U.S. Air Force, Aug. 1981. (Available from DTIC as AD A110 037.)

6. Middleton, W. D.; and Lundry, J. L.: A System for Aerodynamic Design and Analysis of Supersonic Aircraft. Part 1 - General Description and Theoretical Development. NASA CR-3351, 1980.

7. Middleton W. D.; Lundry, J. L.; and Coleman, R. G.: A System for Aerodynamic Design and Analysis of Supersonic Aircraft. Part 2 - User's Manual. NASA CR-3352, 1980.

8. Middleton, W. D.; Lundry, J. L.; and Coleman, R. G.: A System for Aerodynamic Design and Analysis of Supersonic Aircraft. Part 3 - Computer Program Description. NASA CR-3353, 1980.

9. Middleton, W. D.; and Lundry, J. L.: A System for Aerodynamic Design and Analysis of Supersonic Aircraft. Part 4 - Test Cases. NASA CR-3354, 1980.

10. Frink, Neal T.; and Lamar, John E.: Water-Tunnel and Analytical Investigation of the Effect of Strake Design Variables on Strake Vortex Breakdown Characteristics. NASA TP-1676, 1980.

11. Fox, Charles H., Jr.; and Huffman, Jarrett K.: Calibration and Test Capabilities of the Langley 7- by 10-Foot High Speed Tunnel. NASA TM X-74027, 1977.

12. Gillis, Clarence L.; Polhamus, Edward C.; and Gray, Joseph L., Jr.: Charts for Determining Jet-Boundary Corrections for Complete Models in 7- by 10-Foot Closed Rectangular Wind Tunnels. NACA WR L-123, 1945. (Formerly NASA ARR L5G31.)

13. Herriott, John G.: Blockage Corrections for Three-Dimensional-Flow Closed-Throat Wind Tunnels, With Consideration of the Effect of Compressibililty. NACA Rep. 995, 1950.

TABLE I.- GEOMETRIC CHARACTERISTICS OF MODEL

Wing (based on trapezoid extended to fuselage centerline):	
Aspect ratio	3.28
Forward sweep of leading edge, deg	20.233
Forward sweep of trailing edge, deg	49.183
Forward sweep of quarter-chord line, deg	29.505
Taper ratio	0.2142
Area, m^2 (ft^2)	0.139 (1.50)
Span, cm (in.)	67.686 (26.648)
Mean aerodynamic chord, cm (in.)	23.518 (9.259)
Wing spanwise station of mean aerodynamic chord, cm (in.)	13.272 (5.225)
Fuselage station of 25-percent wing mean aerodynamic chord, cm (in.)	62.93 (24.77)
Root chord (at fuselage centerline), cm (in.)	33.993 (13.383)
Tip chord, cm (in.)	7.282 (2.867)
Dihedral, deg	0
Twist (wash in from root to tip), deg	6.0
Incidence (root), deg	-2.0
Airfoil section	4.44-percent-thick supercritical
Canard (based on trapezoid extended to fuselage centerline):	
Leading-edge sweep, deg	45
Aspect ratio	3.28
Taper ratio	0.214
Area, cm^2 (in^2)	349.1 (54.12)
Span, cm (in.)	33.843 (13.324)
Root chord (at fuselage centerline), cm (in.)	16.995 (6.691)
Tip chord, cm (in.)	3.640 (1.433)
Dihedral, deg	10
Airfoil section	4.44-percent-thick supercritical
Fuselage:	
Base cavity area, cm^2 (in^2)	35.613 (5.52)
Vertical tail (based on exposed area):	
Leading-edge sweep, deg	54
Aspect ratio	1.02
Taper ratio	0.310
Area, cm^2 (in^2)	192.000 (29.76)
Span, cm (in.)	13.970 (5.50)
Root chord, cm (in.)	20.980 (8.26)
Tip chord, cm (in.)	6.502 (2.56)
Airfoil section	4-percent circular-arc biconvex
Strakes (based on exposed area of each strake):	
Width, cm (in.)	6.35 (2.50)
Root chord, cm (in.)	45.212 (17.80)
Slenderness ratio	7.12
Area, cm^2 (in^2)	168.39 (26.10)
Dihedral, deg	3

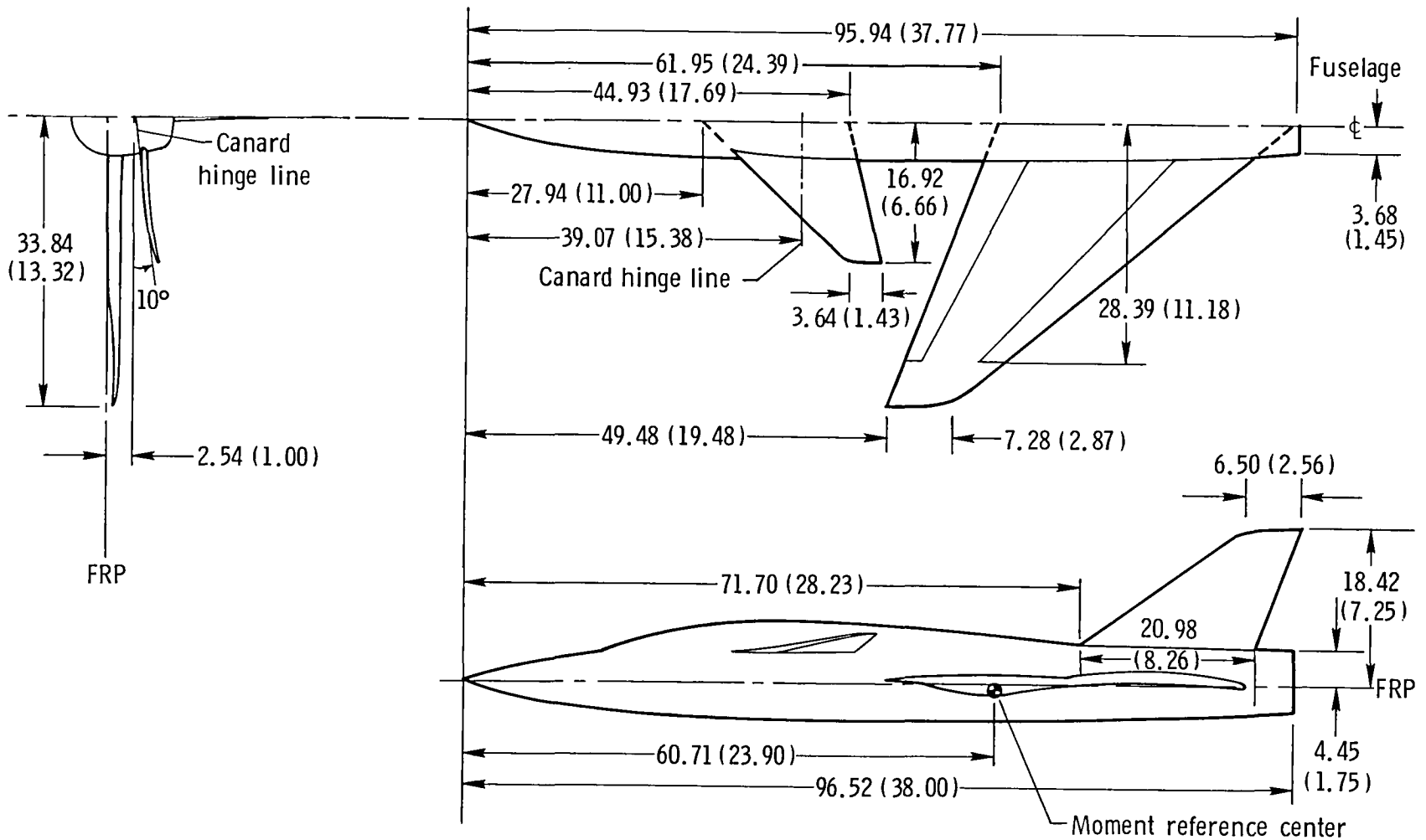

(a) General arrangement of model.

Figure 1.- Geometric characteristics of model. Dimensions are in centimeters (inches).

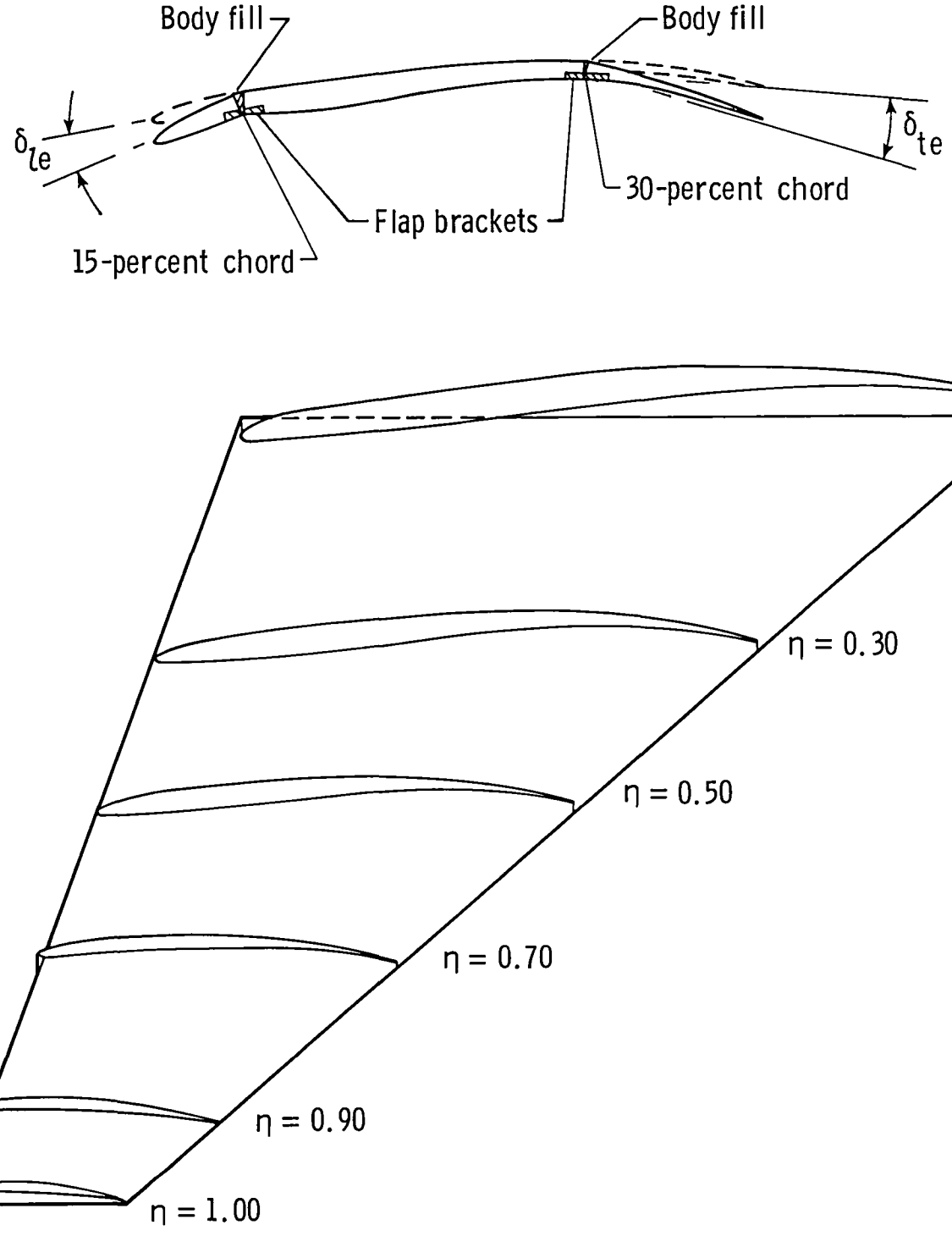

(b) General shapes of wing sections.

Figure 1.- Continued.

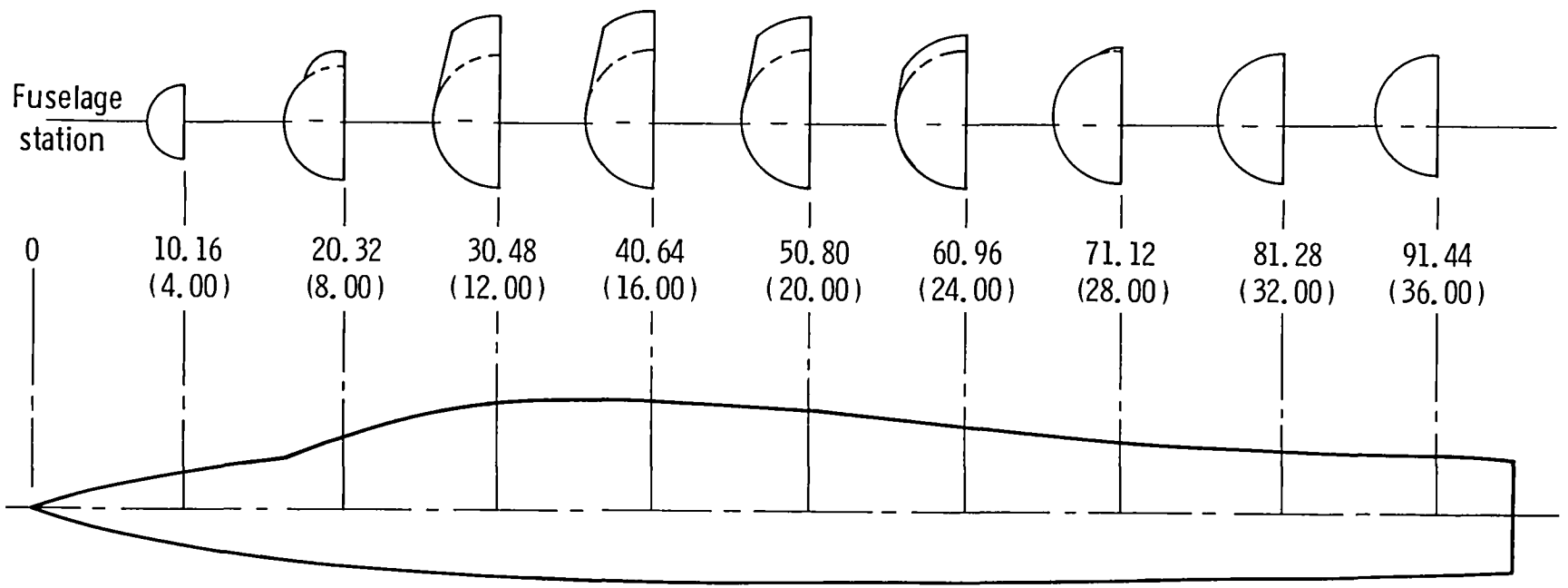

(c) Fuselage cross sections.

Figure 1.- Continued.

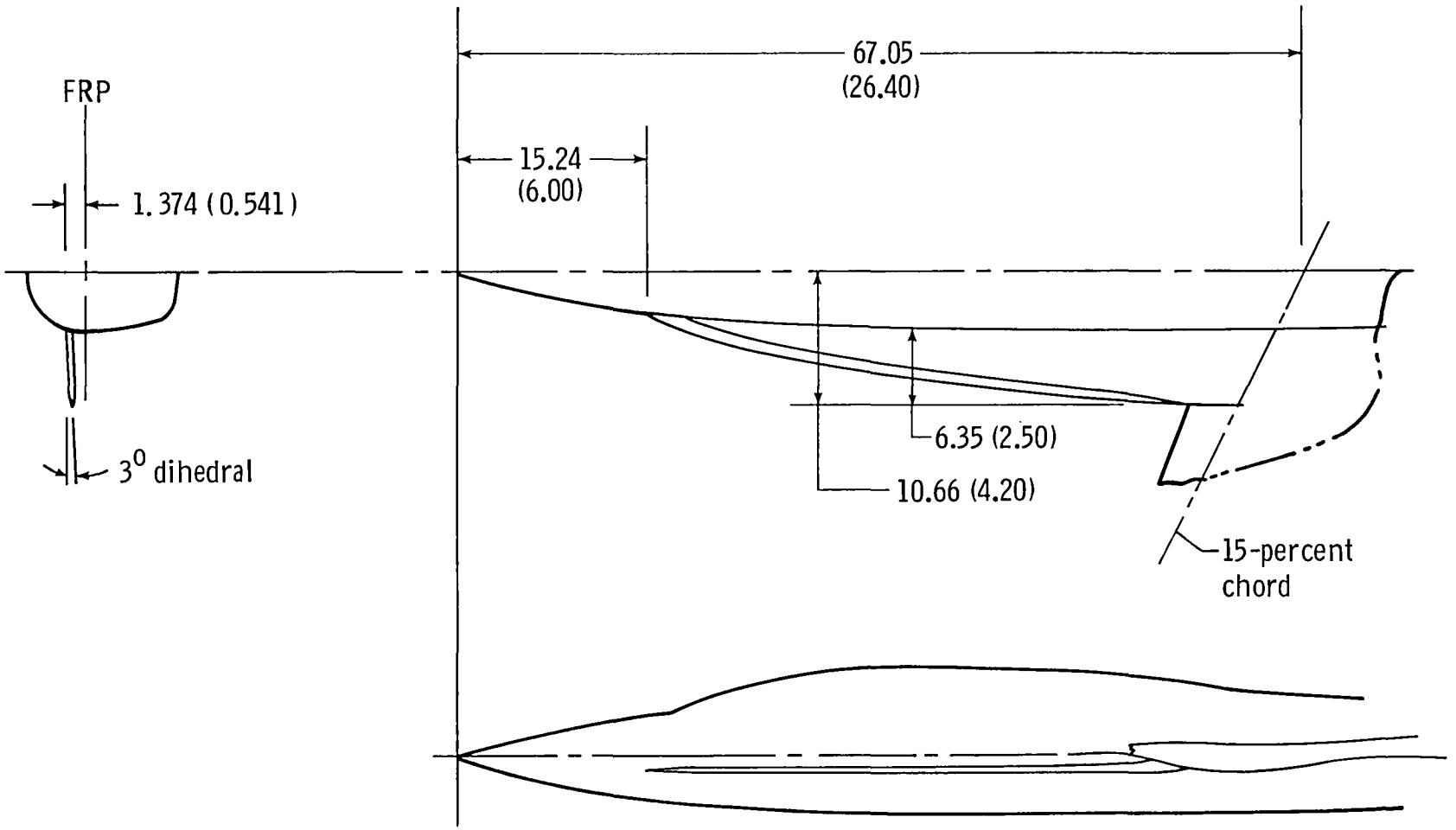

(d) General arrangement of fuselage strakes.

Figure 1.- Concluded.

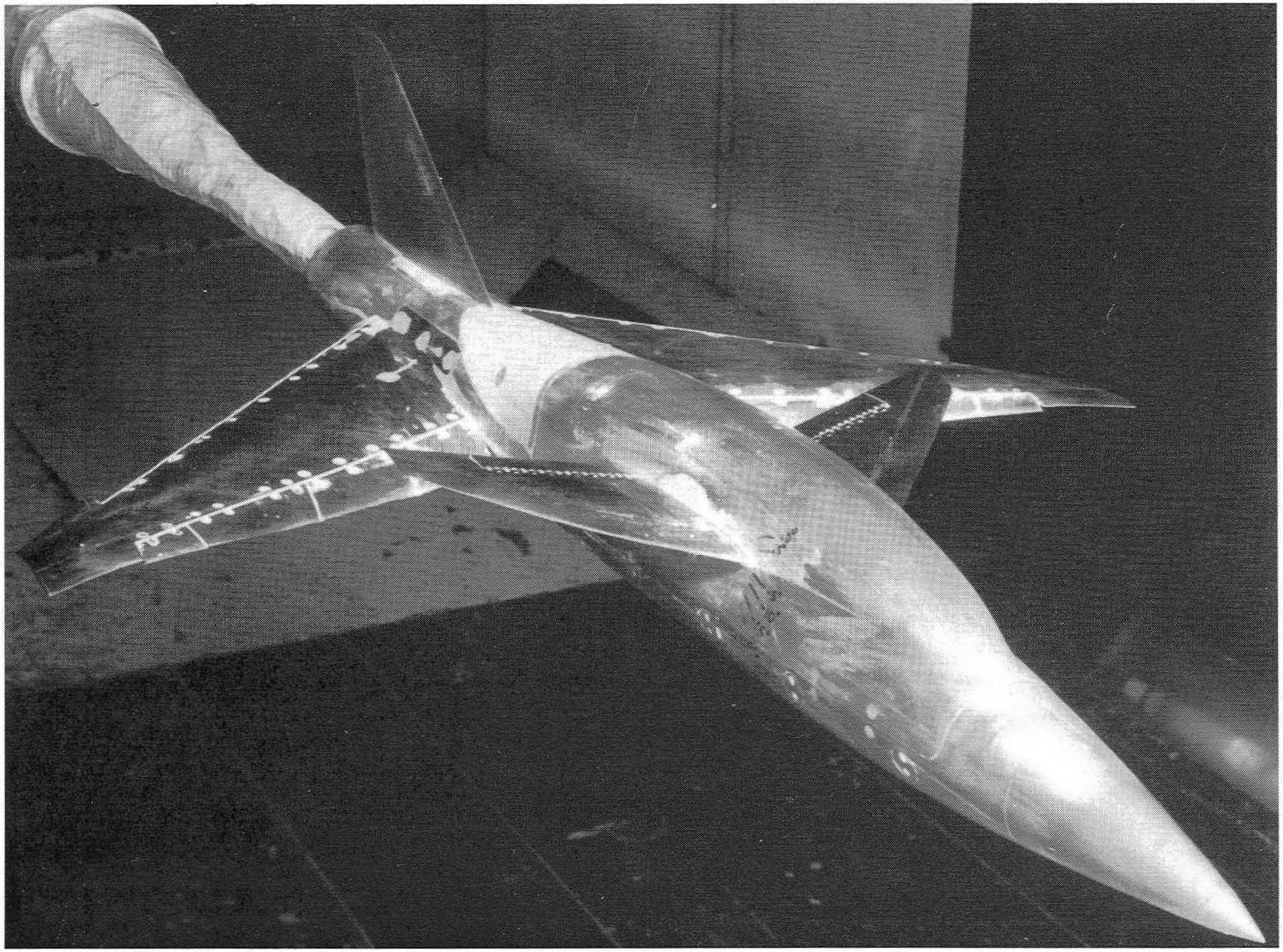

L-83-921

(a) Three-quarter front view of wing-plus-canard configuration.

Figure 2.- Forward-swept wing model installed in Langley 7- by 10-Foot High-Speed Tunnel.

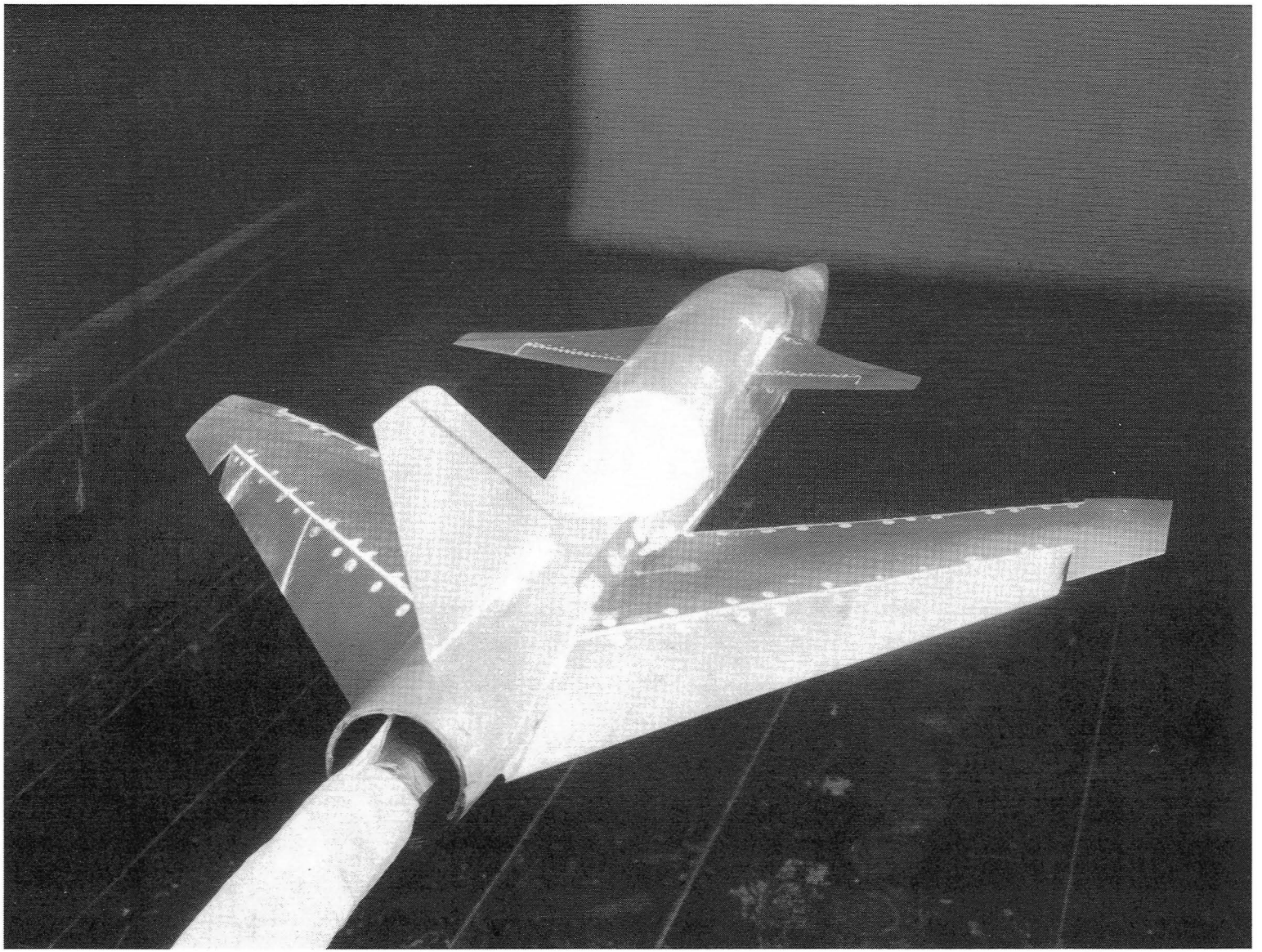

(b) Three-quarter rear view of wing-plus-canard configuration.

Figure 2.- Continued.

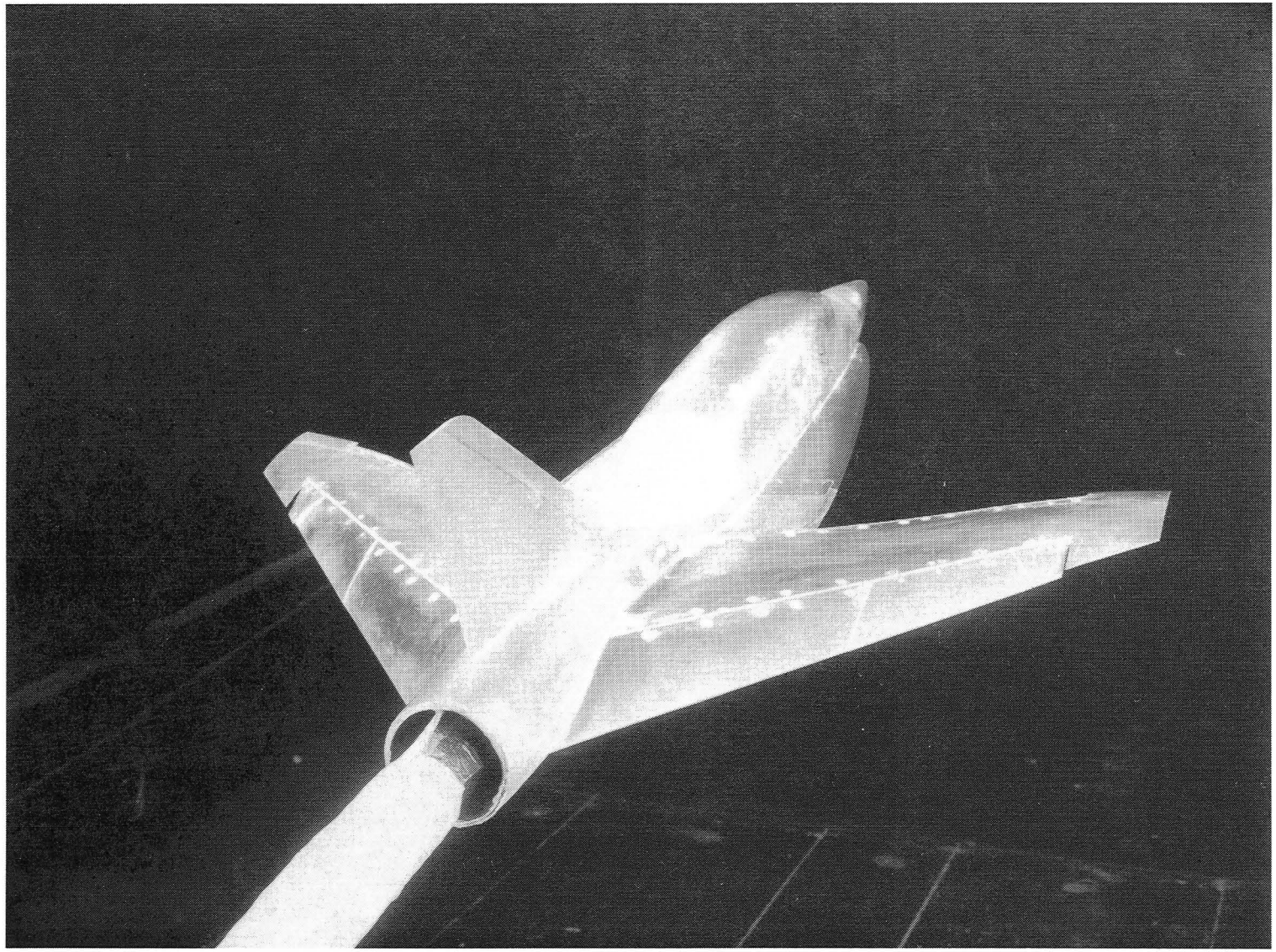

L-83-872

(c) Wing-plus-strakes configuration.

Figure 2.- Continued.

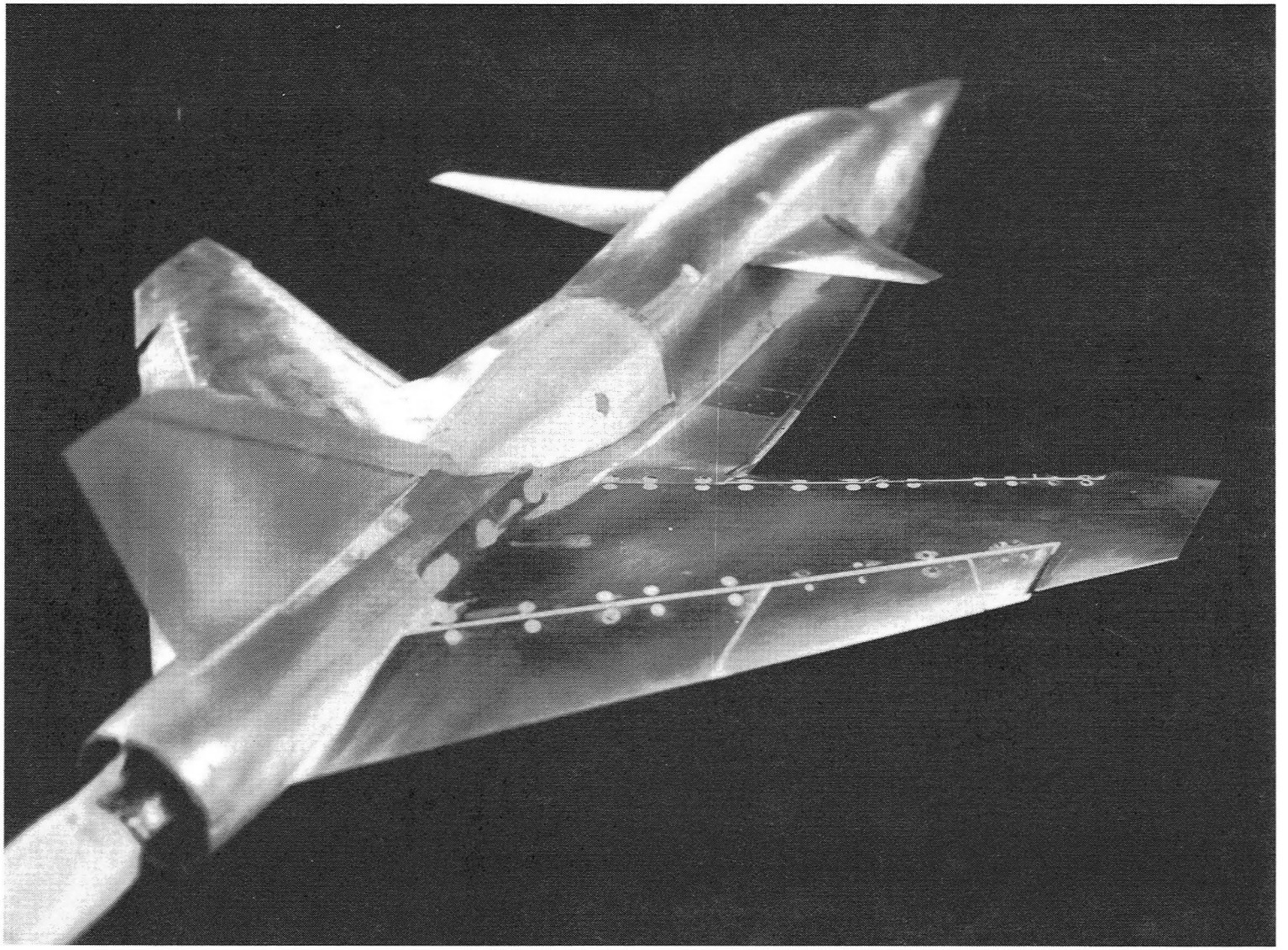

L-83-7269

(d) Wing-plus-canard-plus-strakes configuration.

Figure 2.- Concluded.

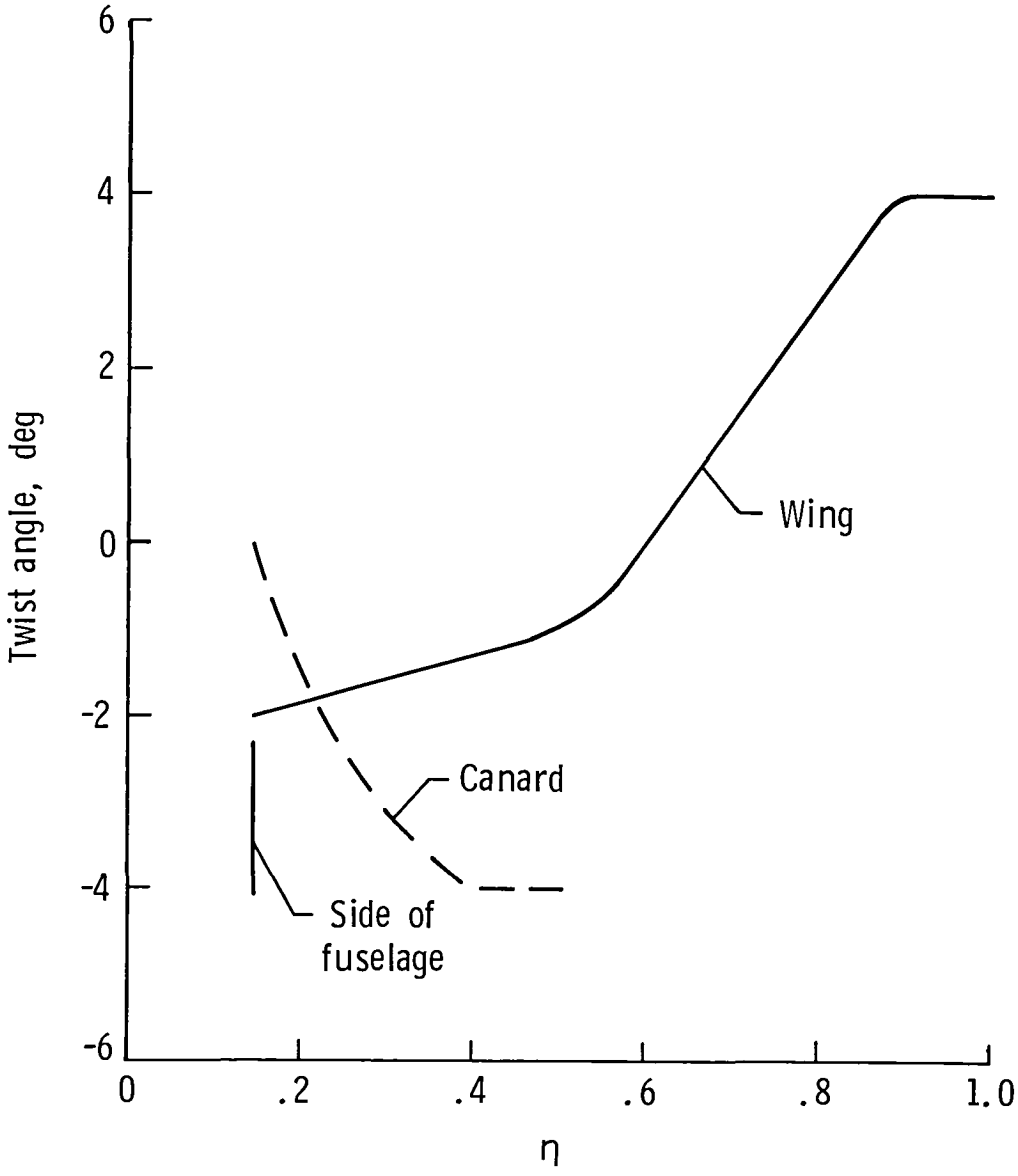

Figure 3.- Wing and canard twist distributions.

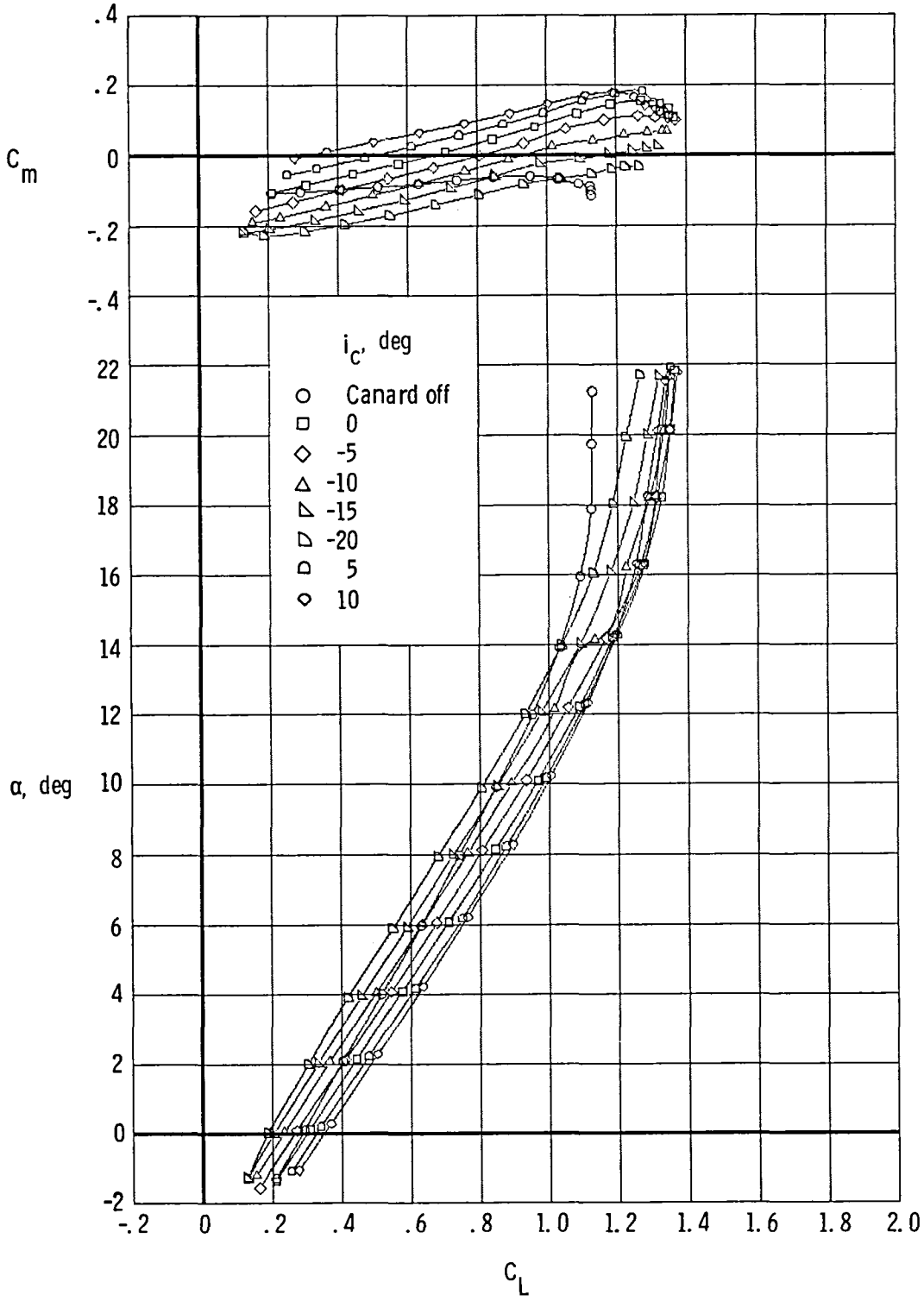

(a) $\delta_{le} = 0°$; $\delta_{te} = 0°$.

Figure 4.- Effects of canard incidence on longitudinal characteristics for different trailing-edge flap deflections.

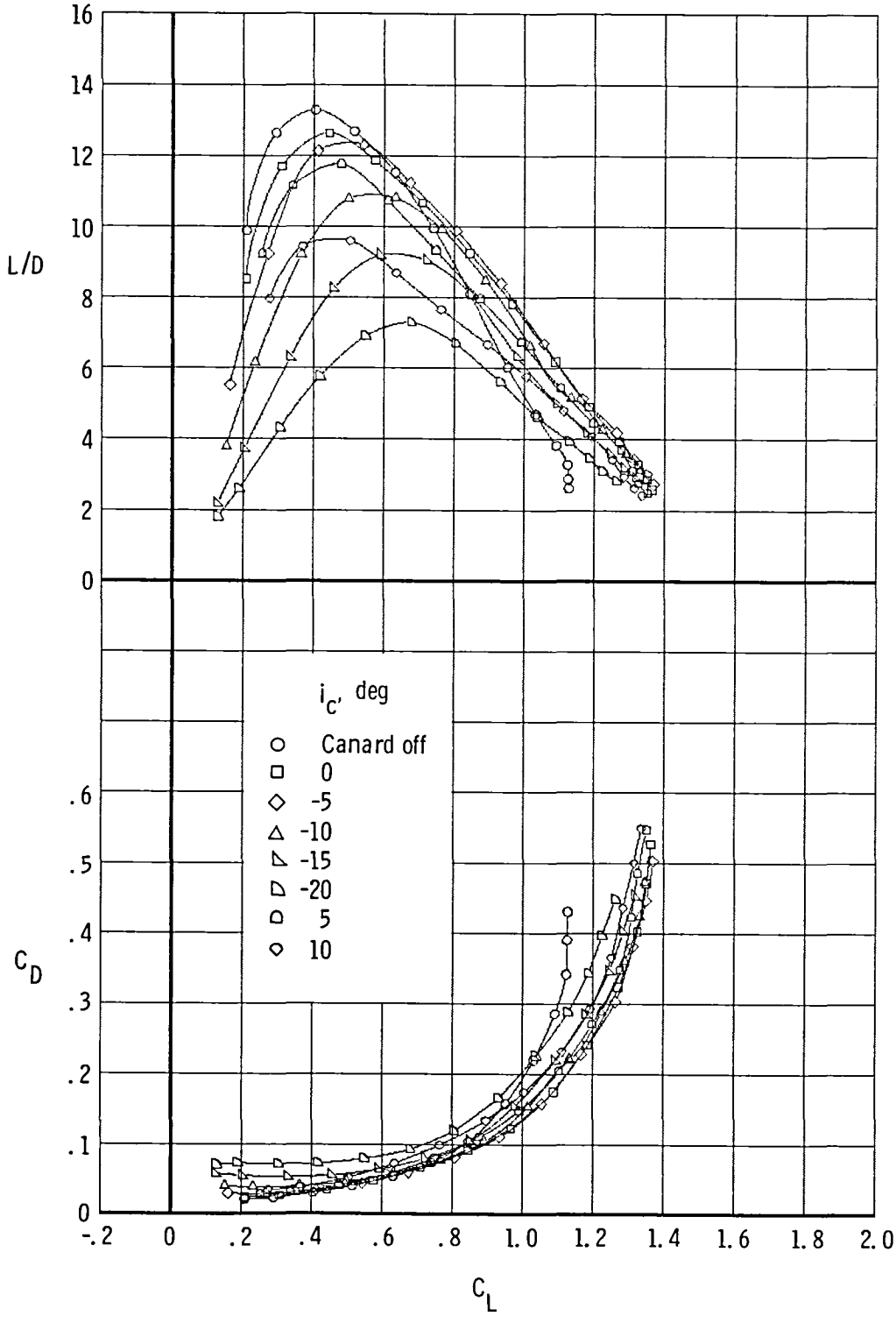

(a) Concluded.

Figure 4.- Continued.

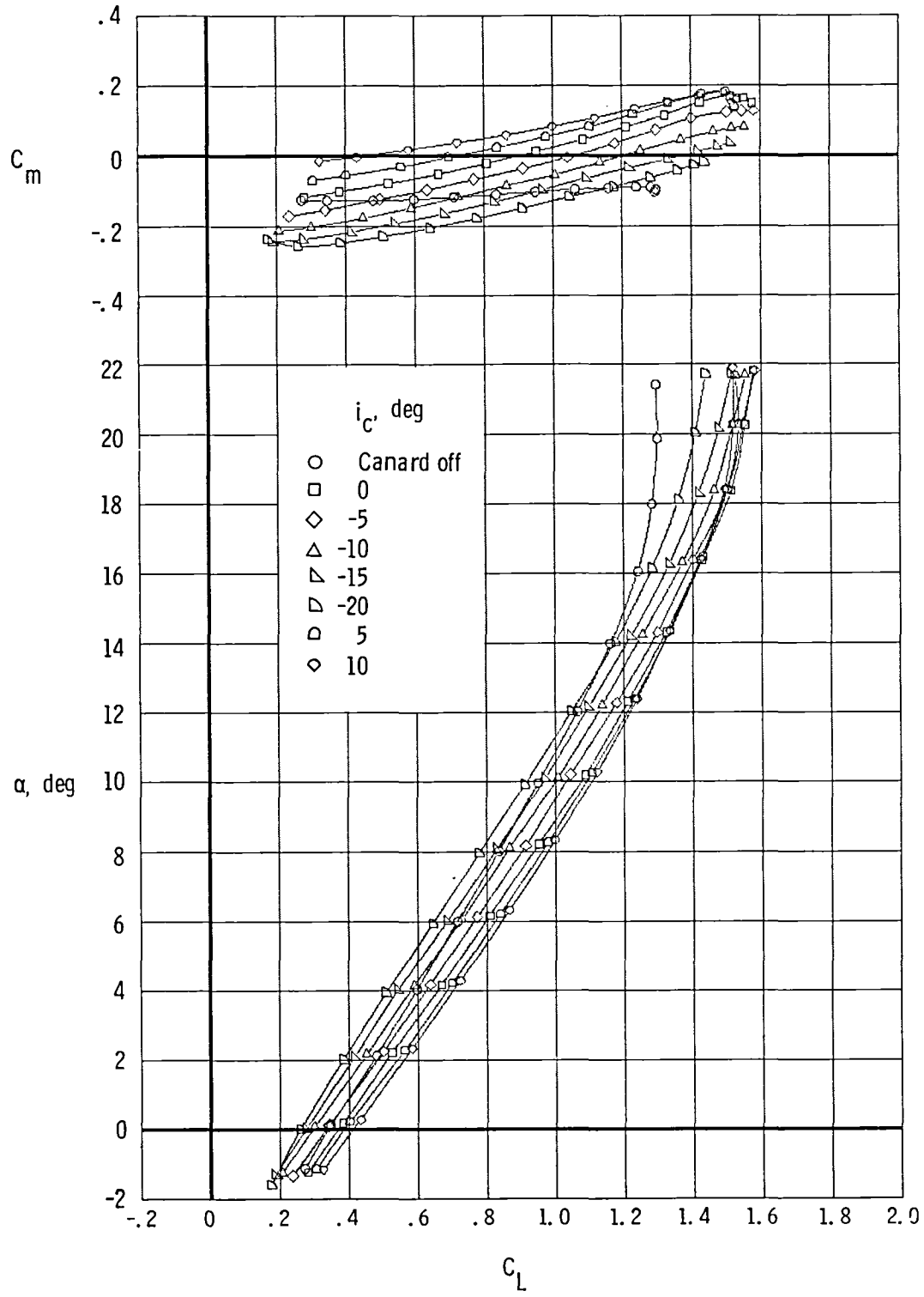

(b) $\delta_{le} = 10°$; $\delta_{te} = 5°$.

Figure 4.- Continued.

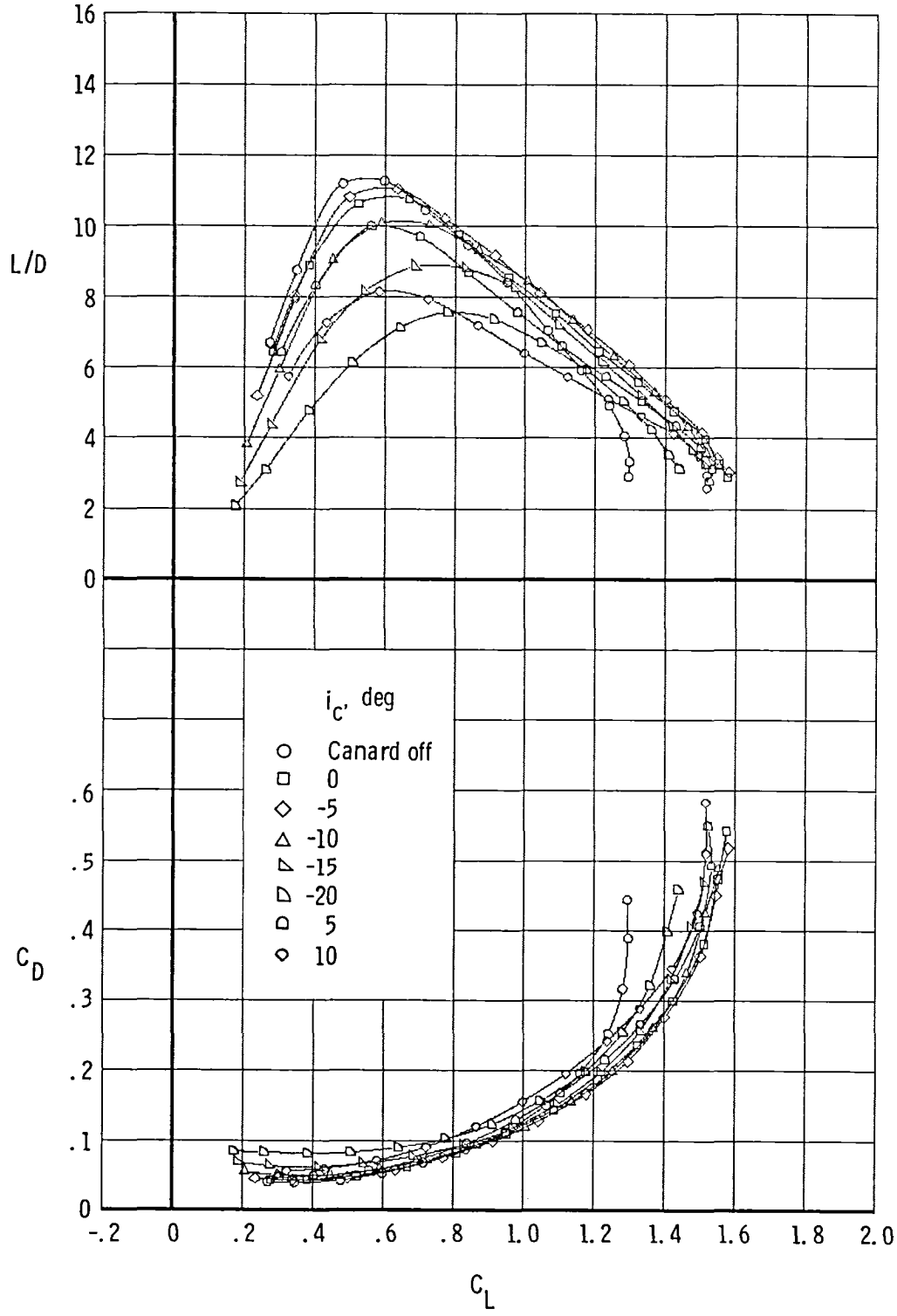

(b) Concluded.

Figure 4.- Continued.

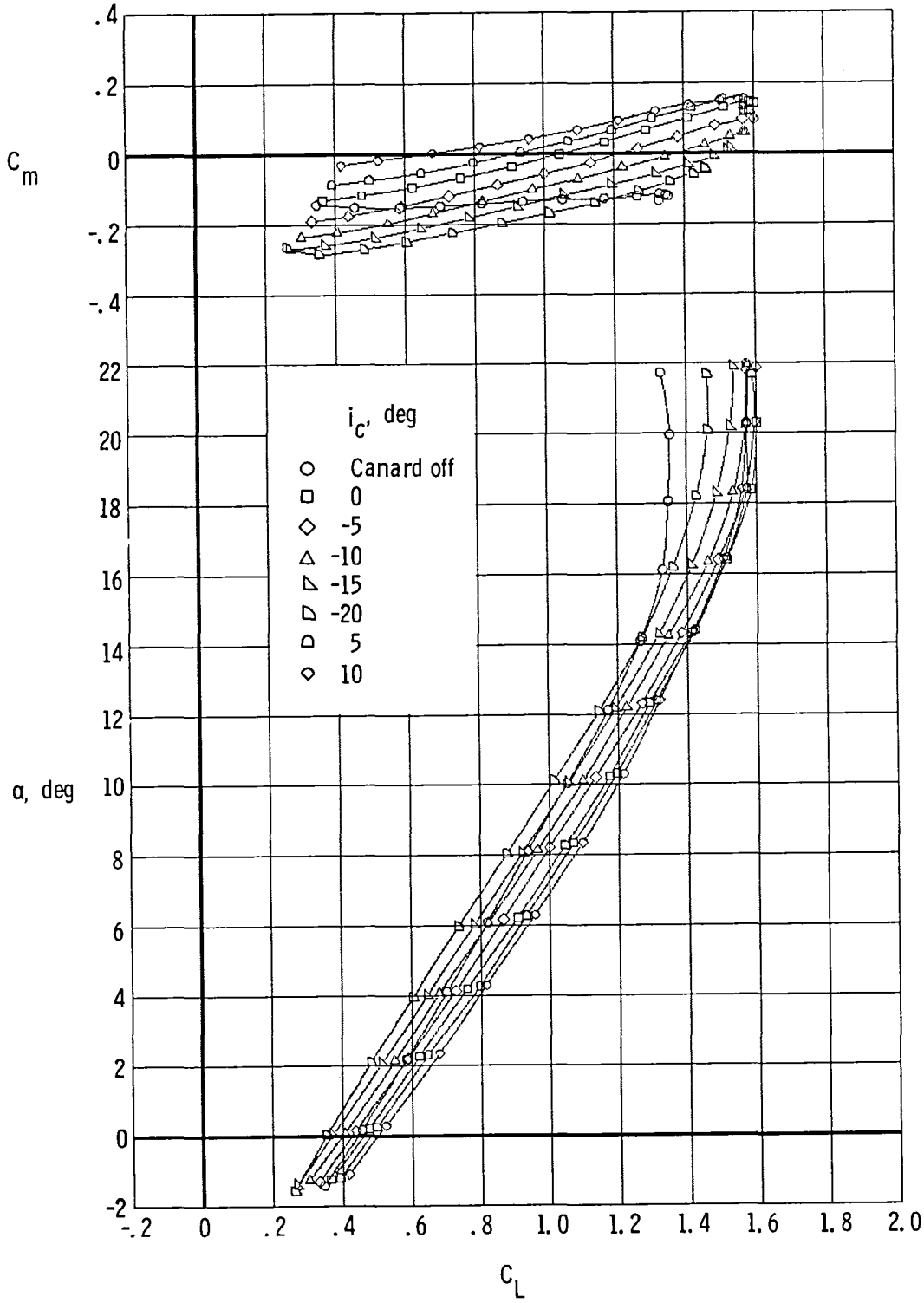

(c) $\delta_{le} = 10°$; $\delta_{te} = 10°$.

Figure 4.- Continued.

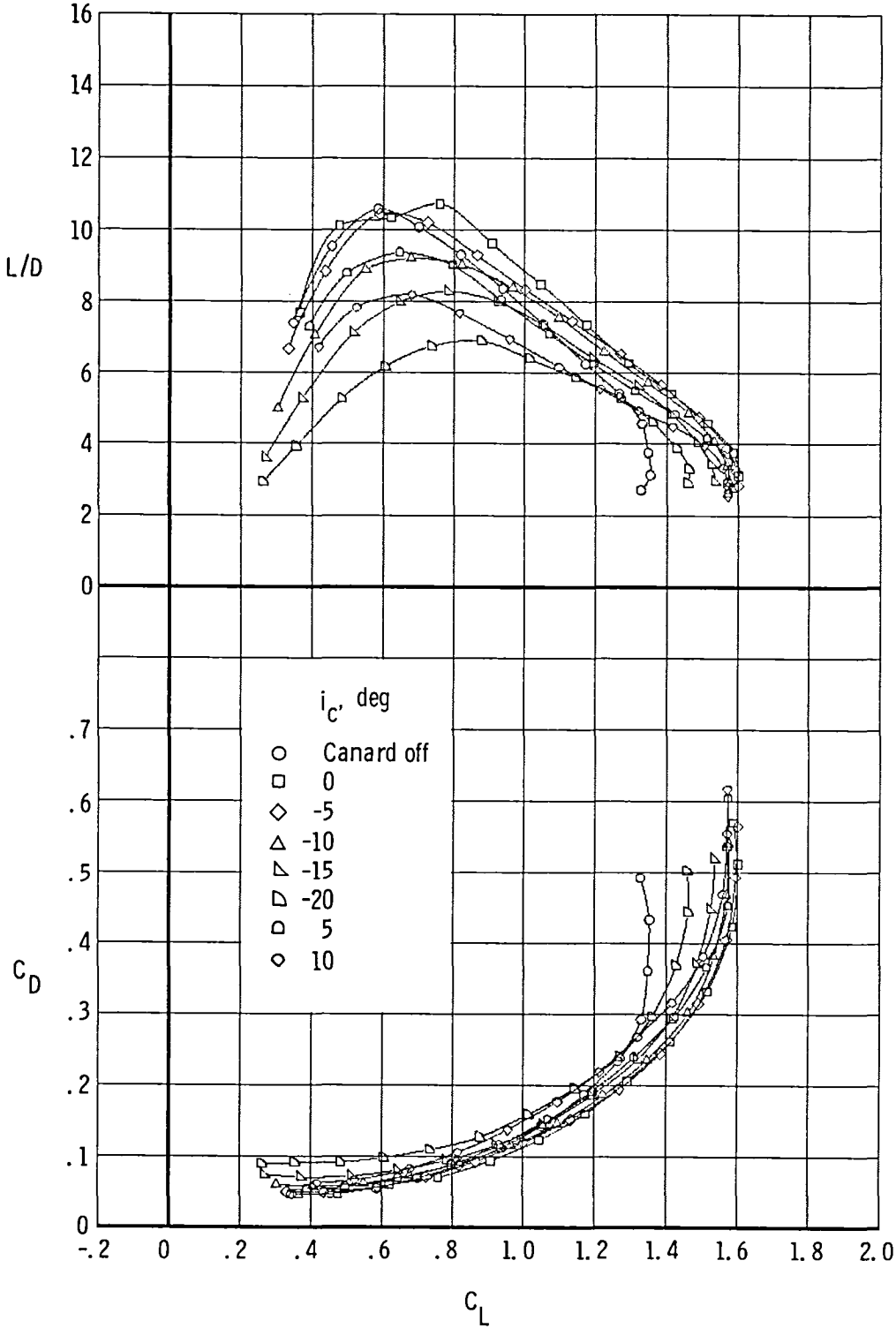

(c) Concluded.

Figure 4.- Continued.

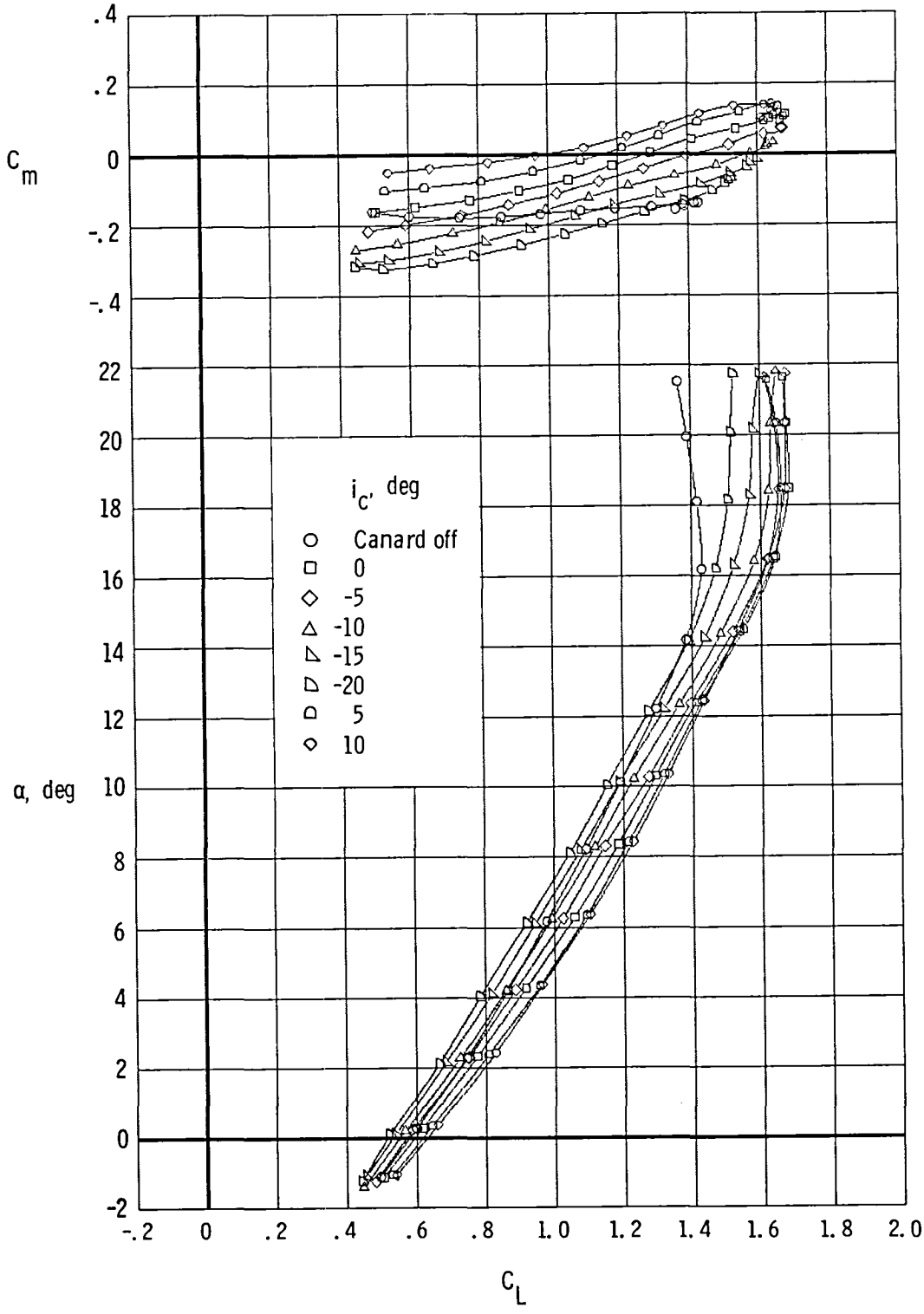

(d) $\delta_{le} = 10°$; $\delta_{te} = 20°$.

Figure 4.- Continued.

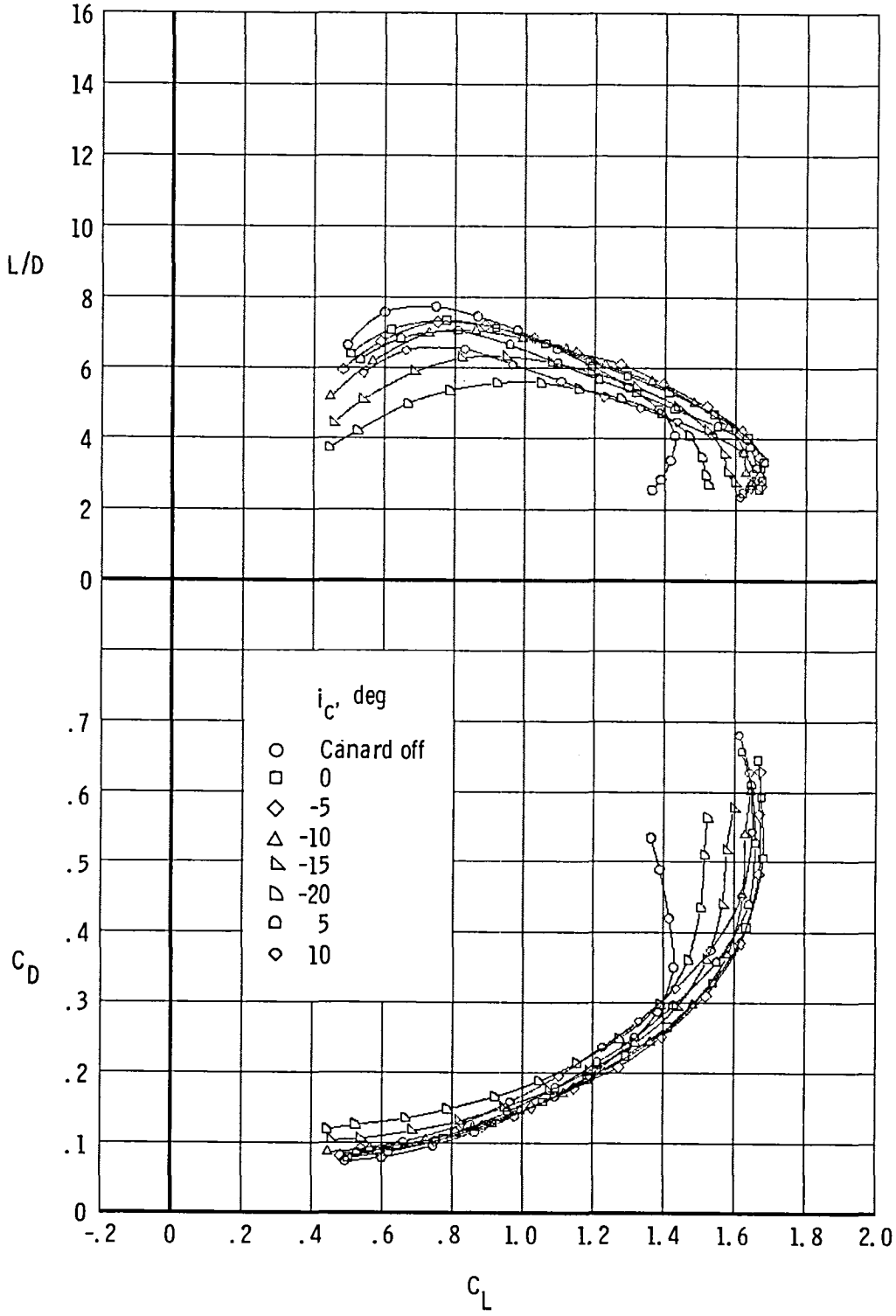

(d) Concluded.

Figure 4.- Concluded.

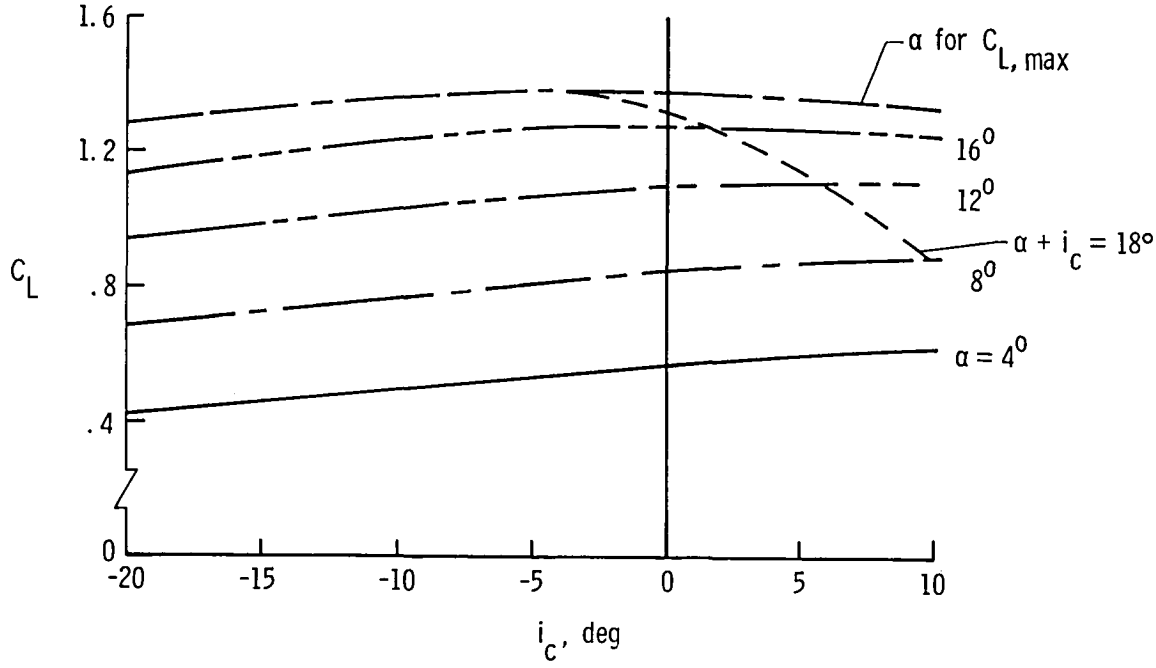

(a) $\delta_{le} = 0°$; $\delta_{te} = 0°$.

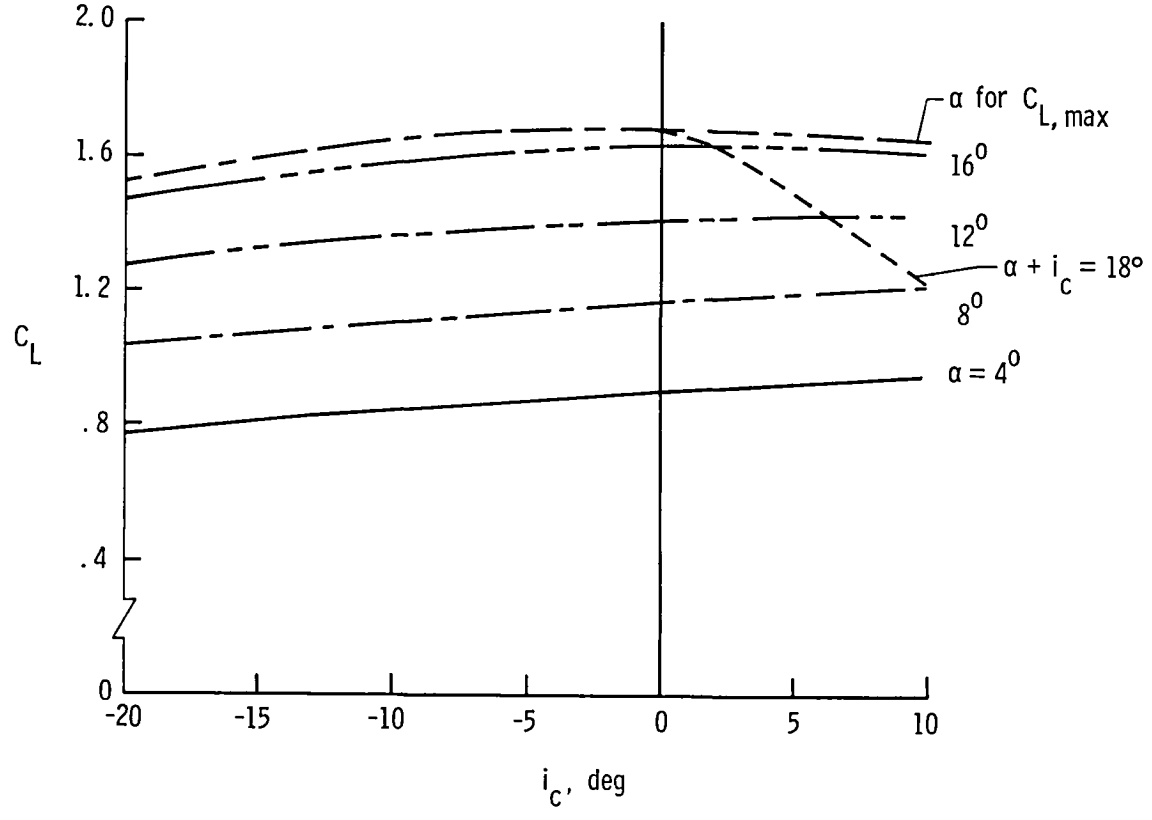

(b) $\delta_{le} = 10°$; $\delta_{te} = 20°$.

Figure 5.- Variation of lift coefficient with canard incidence for various wing angles of attack.

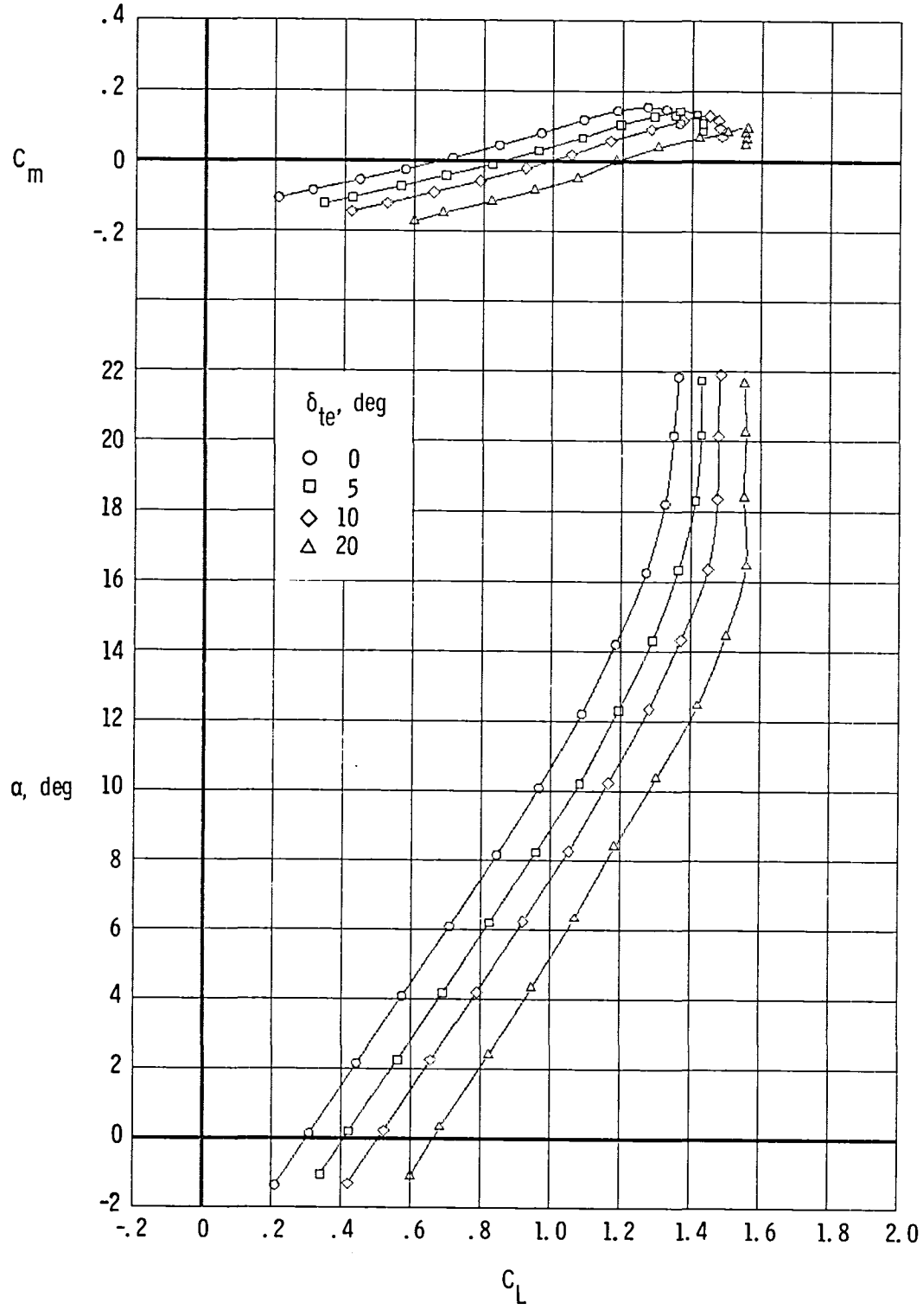

(a) Lift and pitching moment.

Figure 6.- Effects of trailing-edge flap deflection on longitudinal aerodynamic characteristics for $i_c = 0°$ and $\delta_{le} = 0°$.

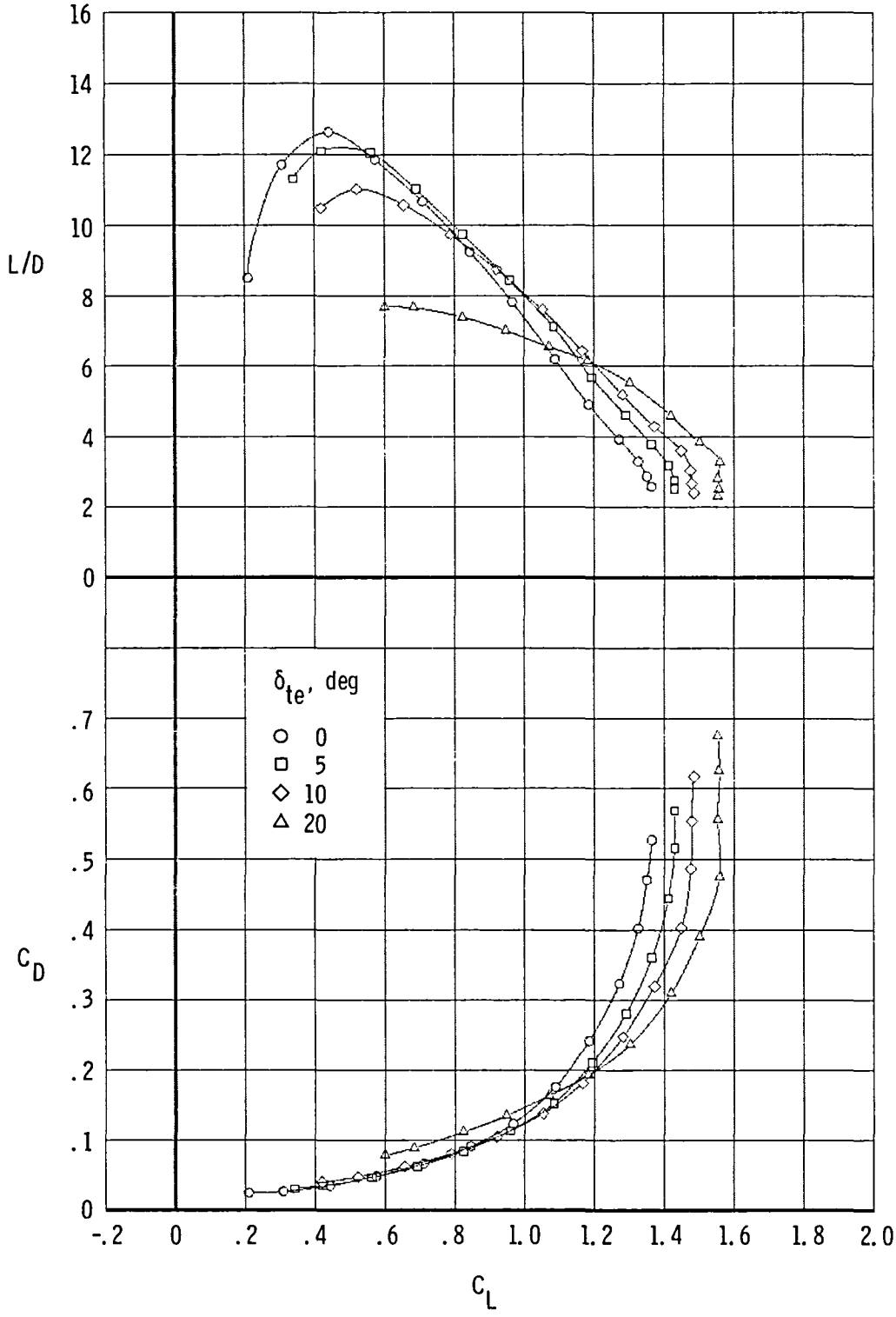

(b) Drag and L/D.

Figure 6.- Concluded.

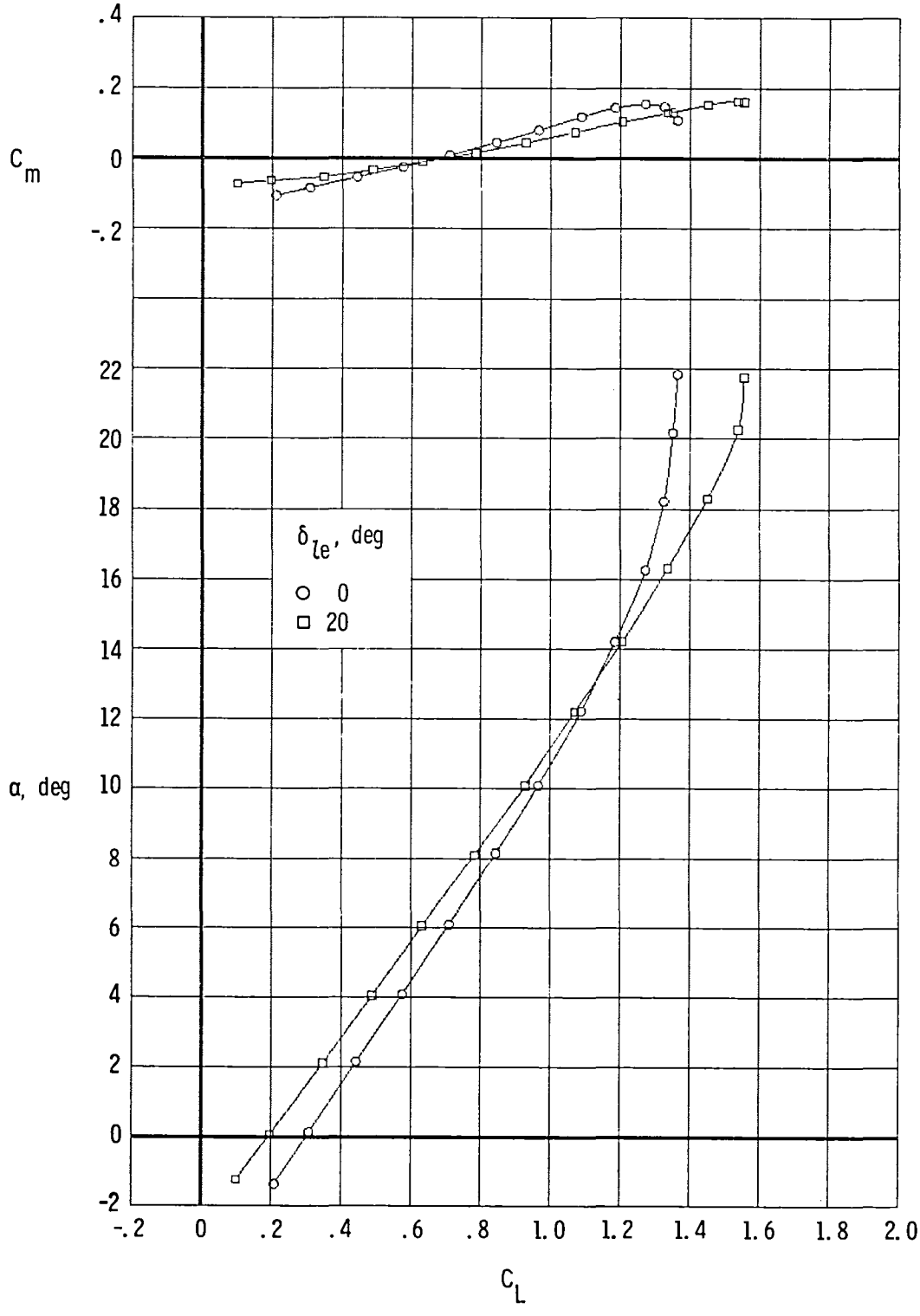

(a) $\delta_{te} = 0°$.

Figure 7.- Effects of leading-edge flap deflection on longitudinal aerodynamic characteristics for different trailing-edge flap deflections and $i_c = 0°$.

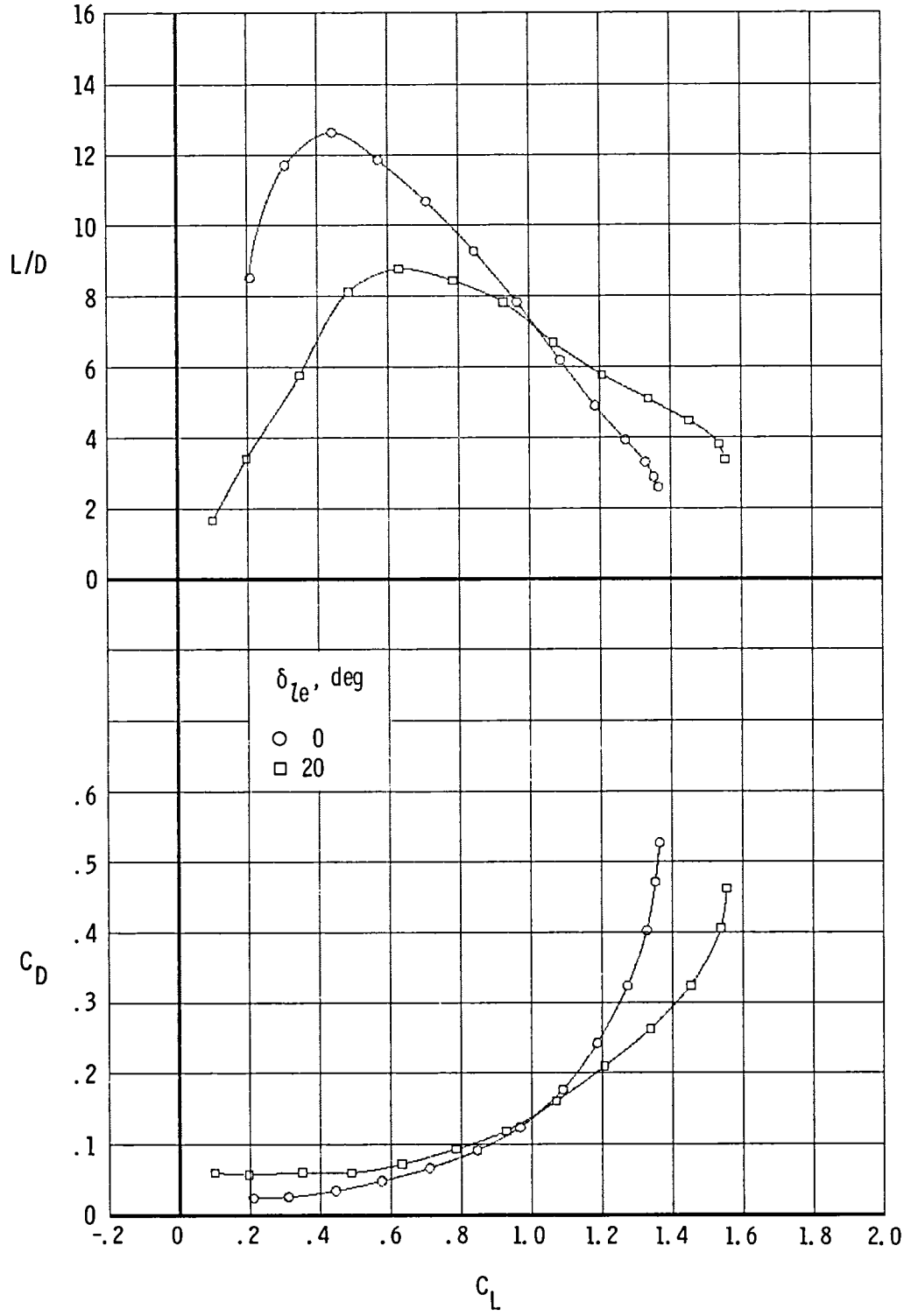

(a) Concluded.

Figure 7.- Continued.

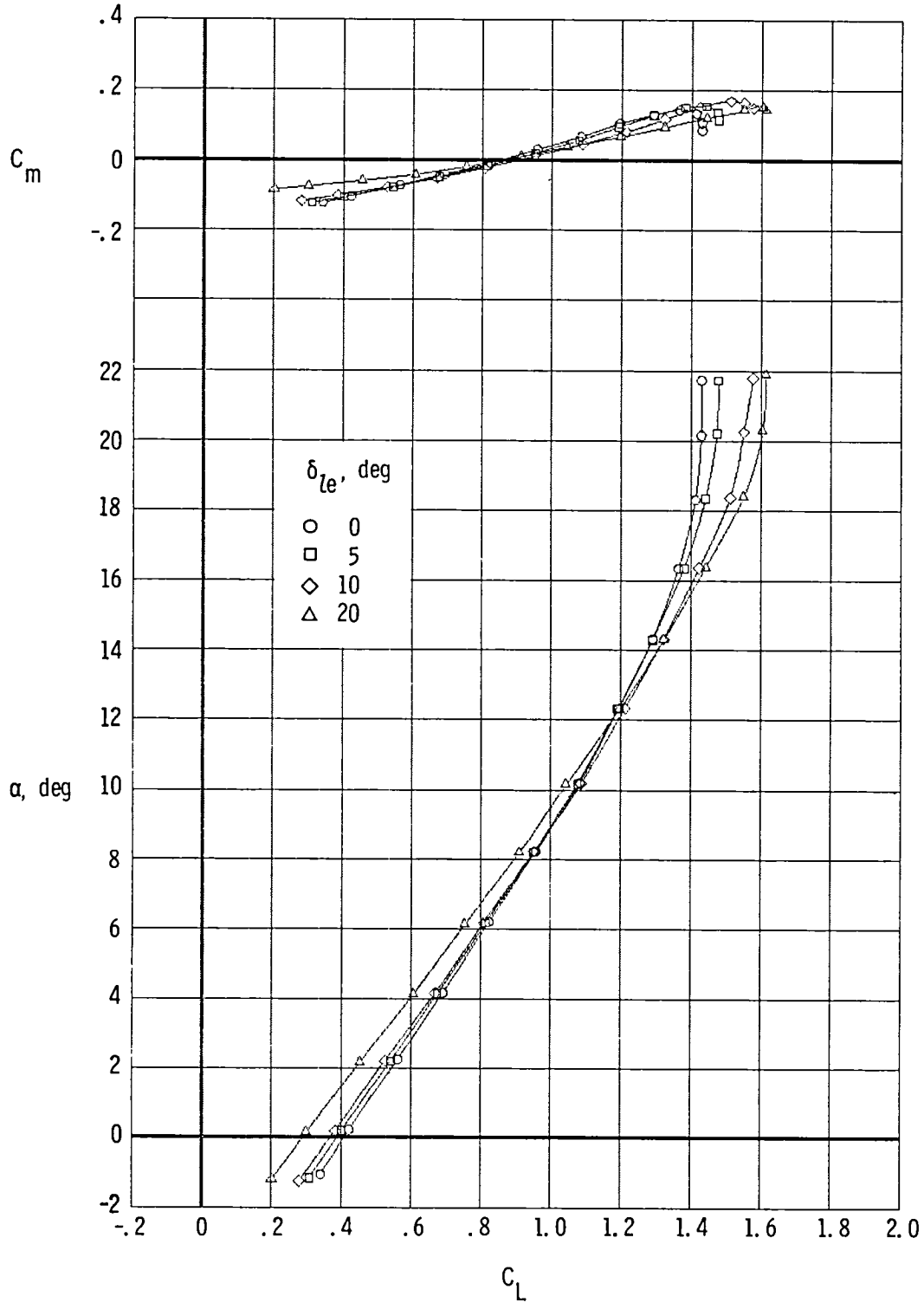

(b) $\delta_{te} = 5°$.

Figure 7.- Continued.

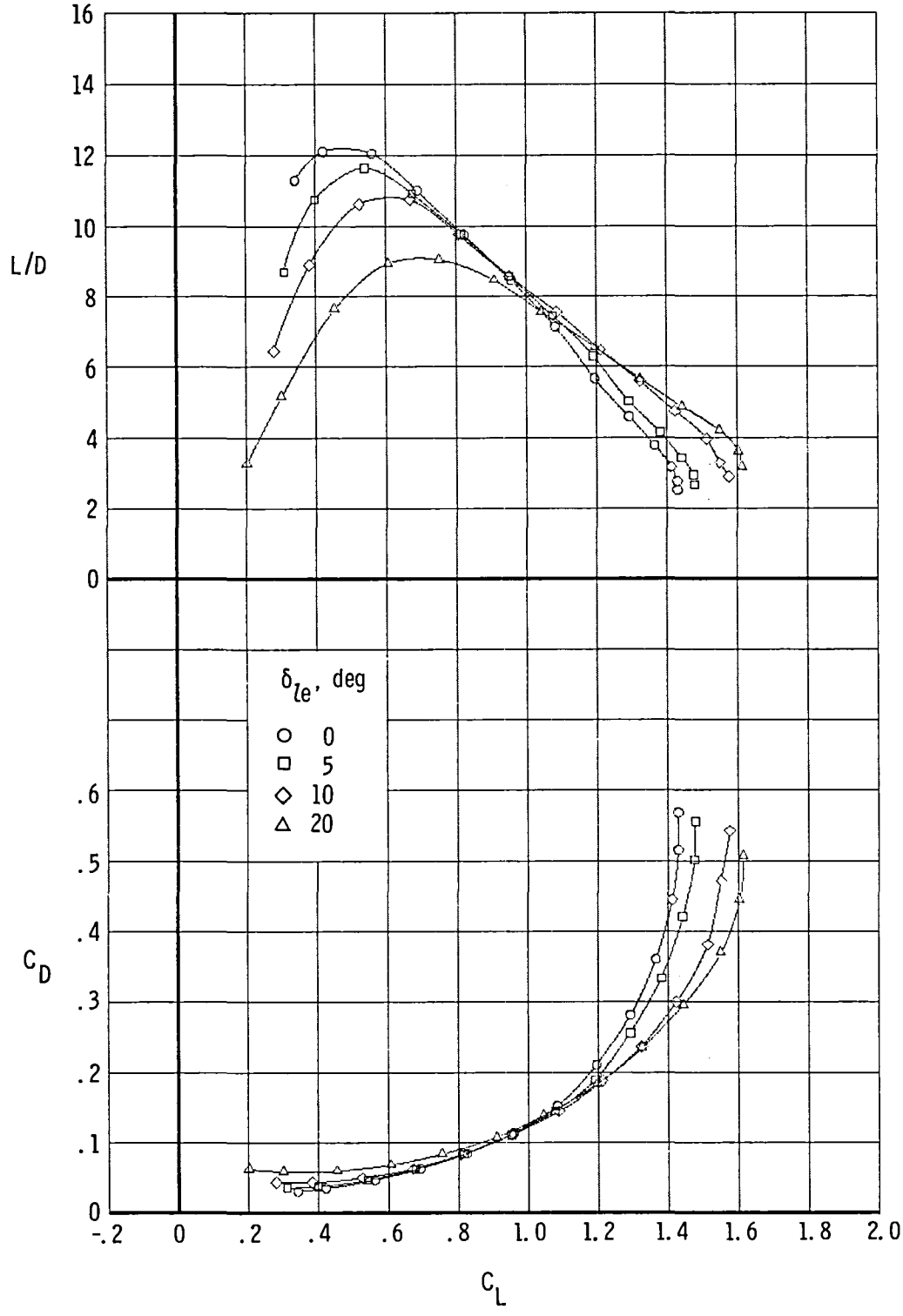

(b) Concluded.

Figure 7.- Continued.

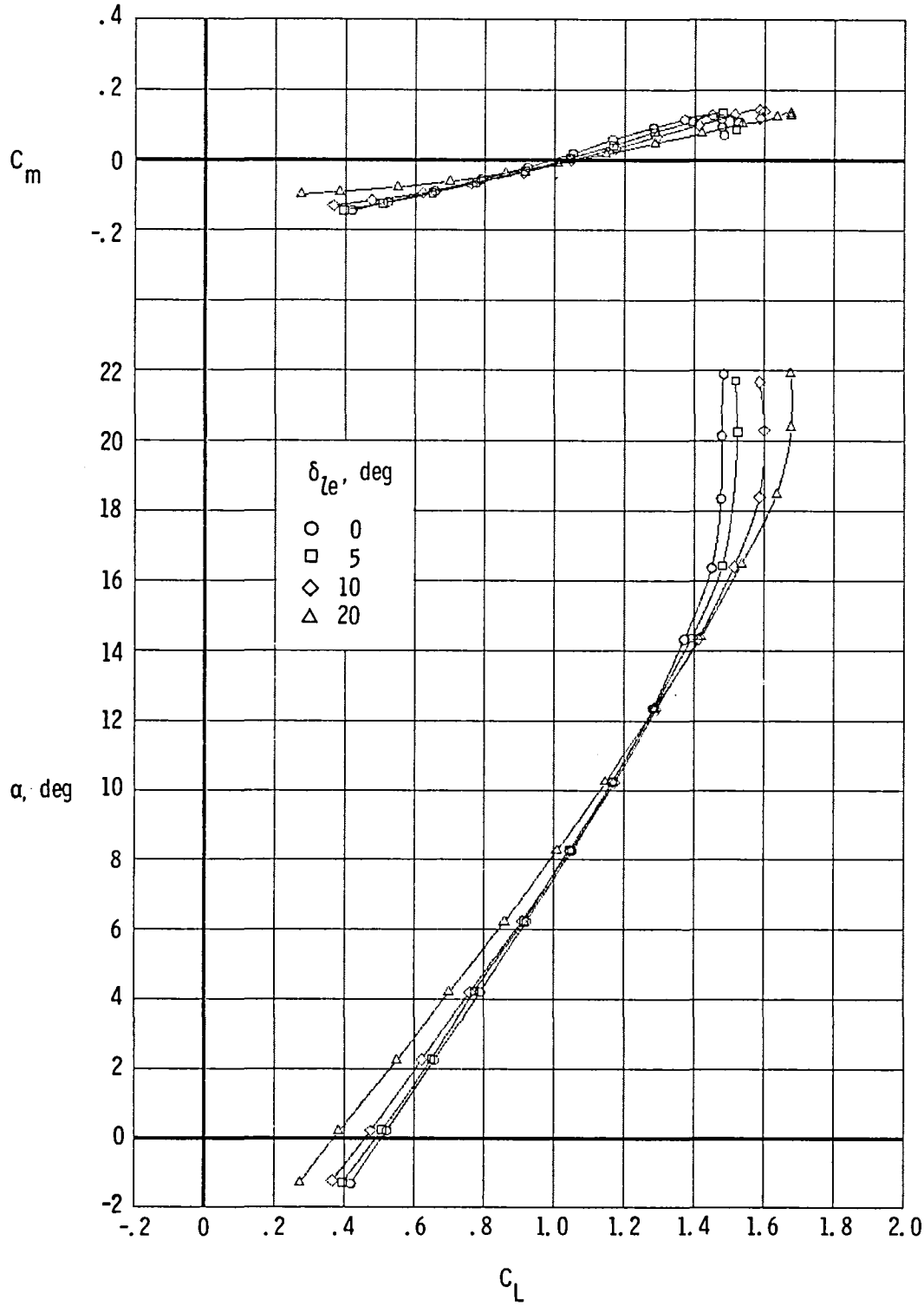

(c) $\delta_{te} = 10°$.

Figure 7.- Continued.

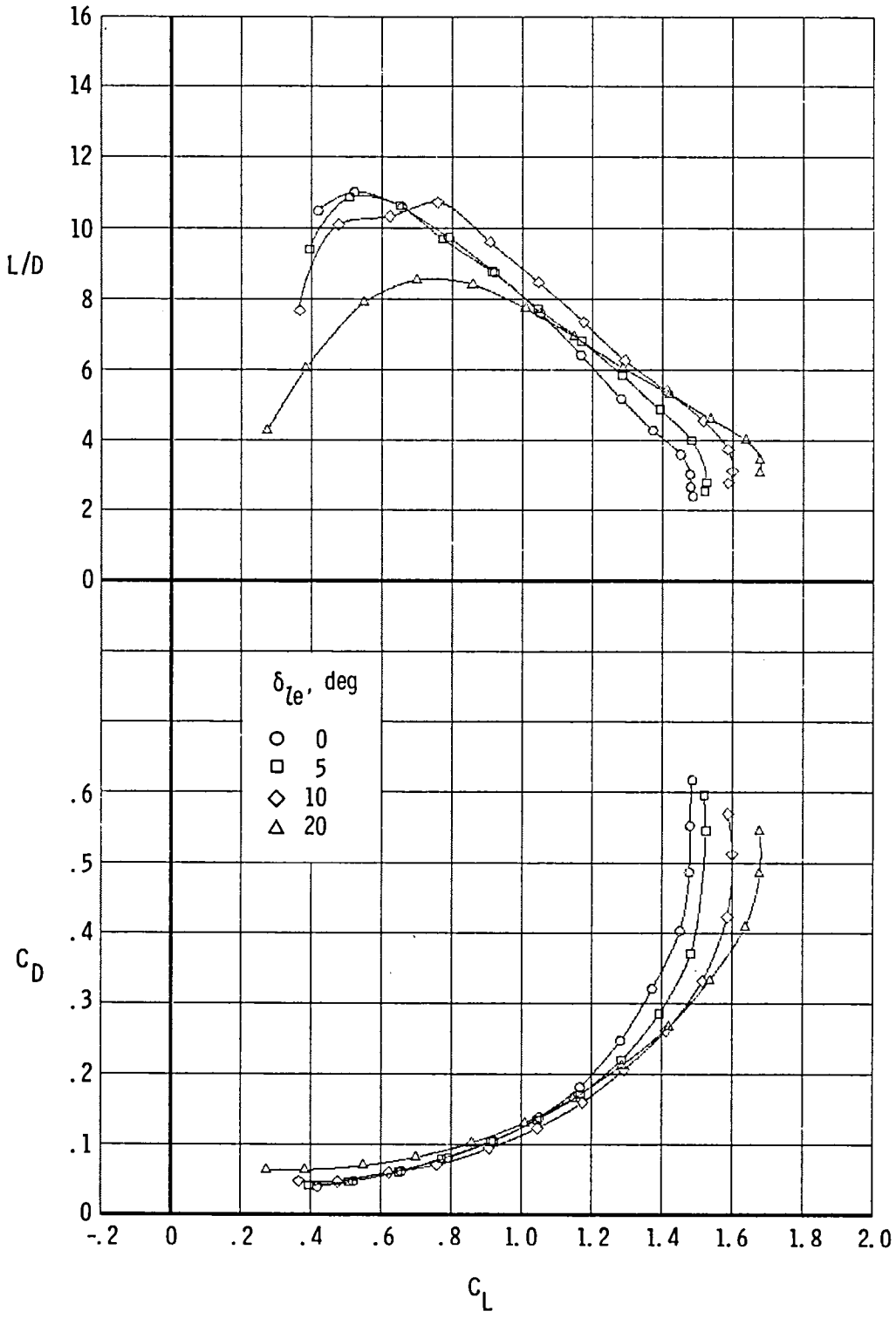

(c) Concluded.

Figure 7.- Continued.

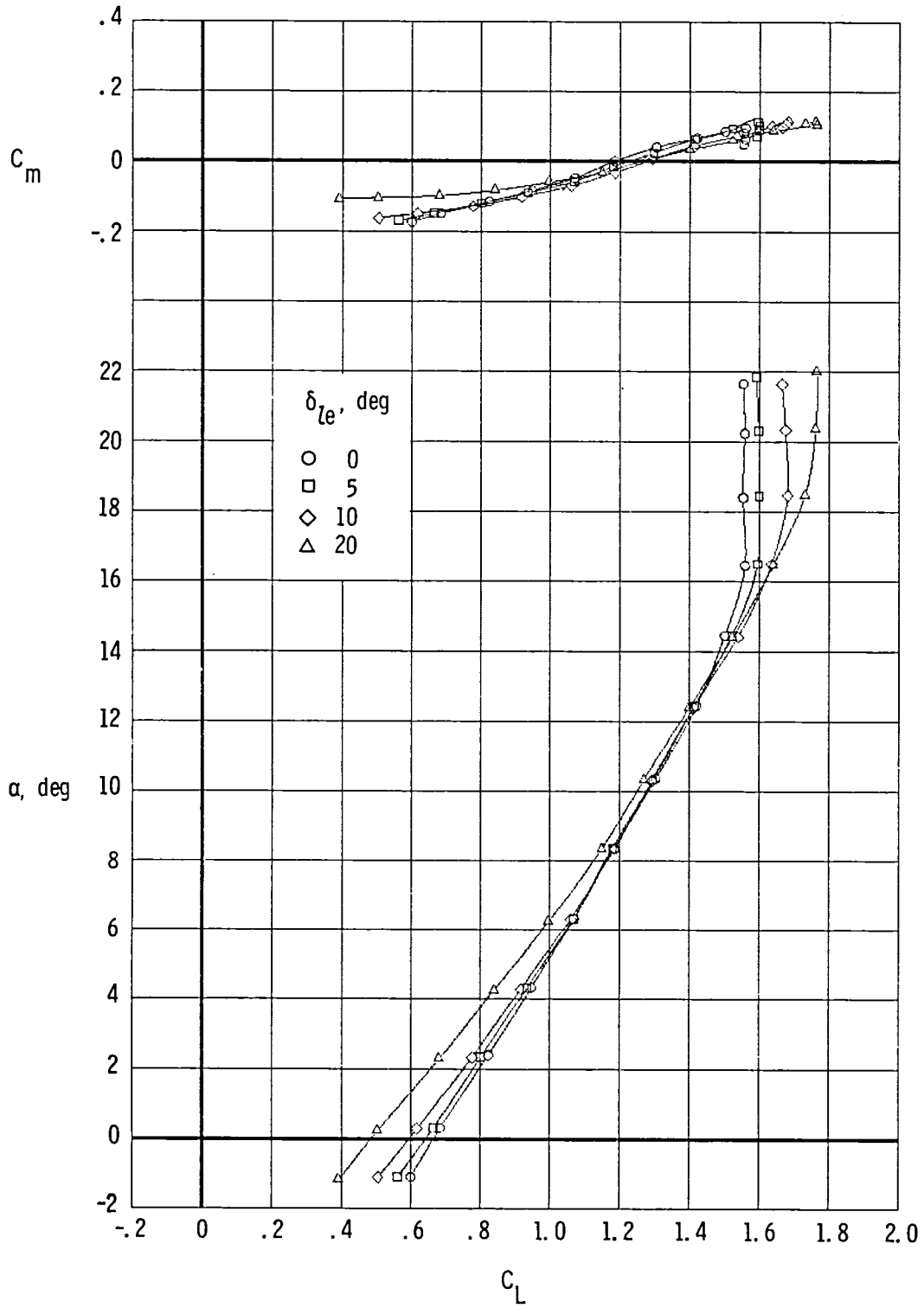

(d) $\delta_{te} = 20°$.

Figure 7.- Continued.

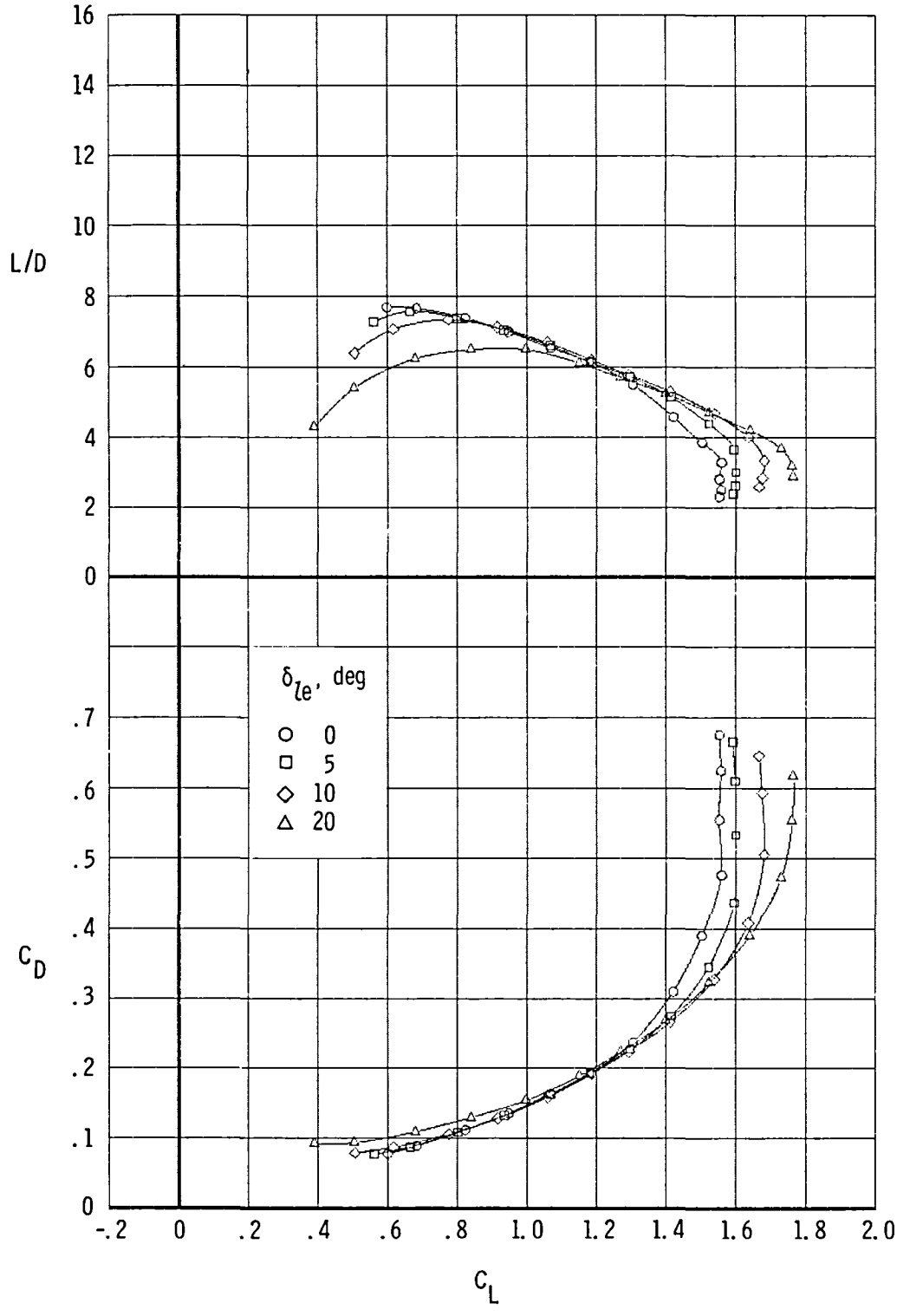

(d) Concluded.

Figure 7.- Concluded.

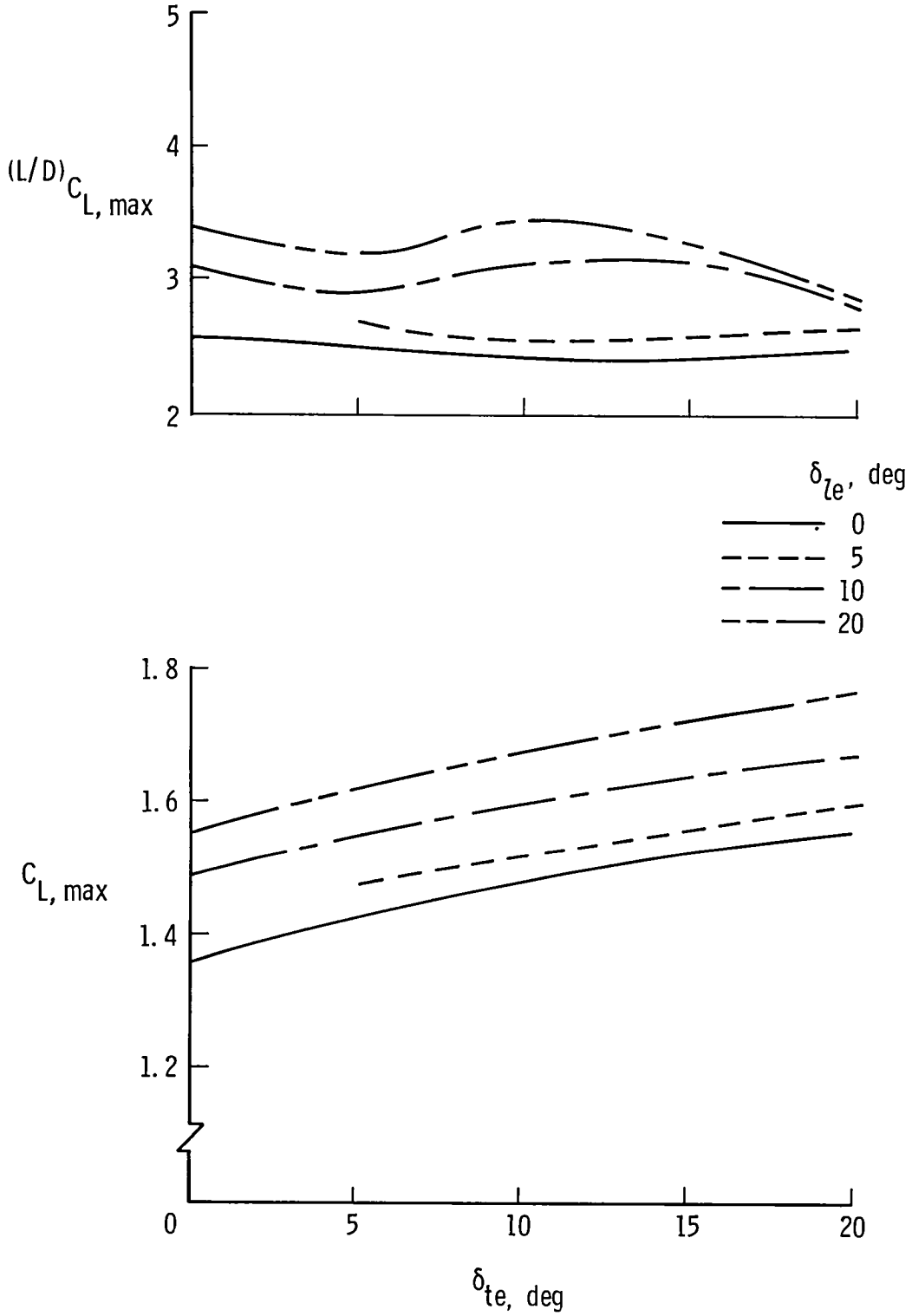

Figure 8.- Effects of leading- and trailing-edge flap deflections on $C_{L,max}$ and $(L/D)_{C_{L,max}}$ with $i_c = 0°$.

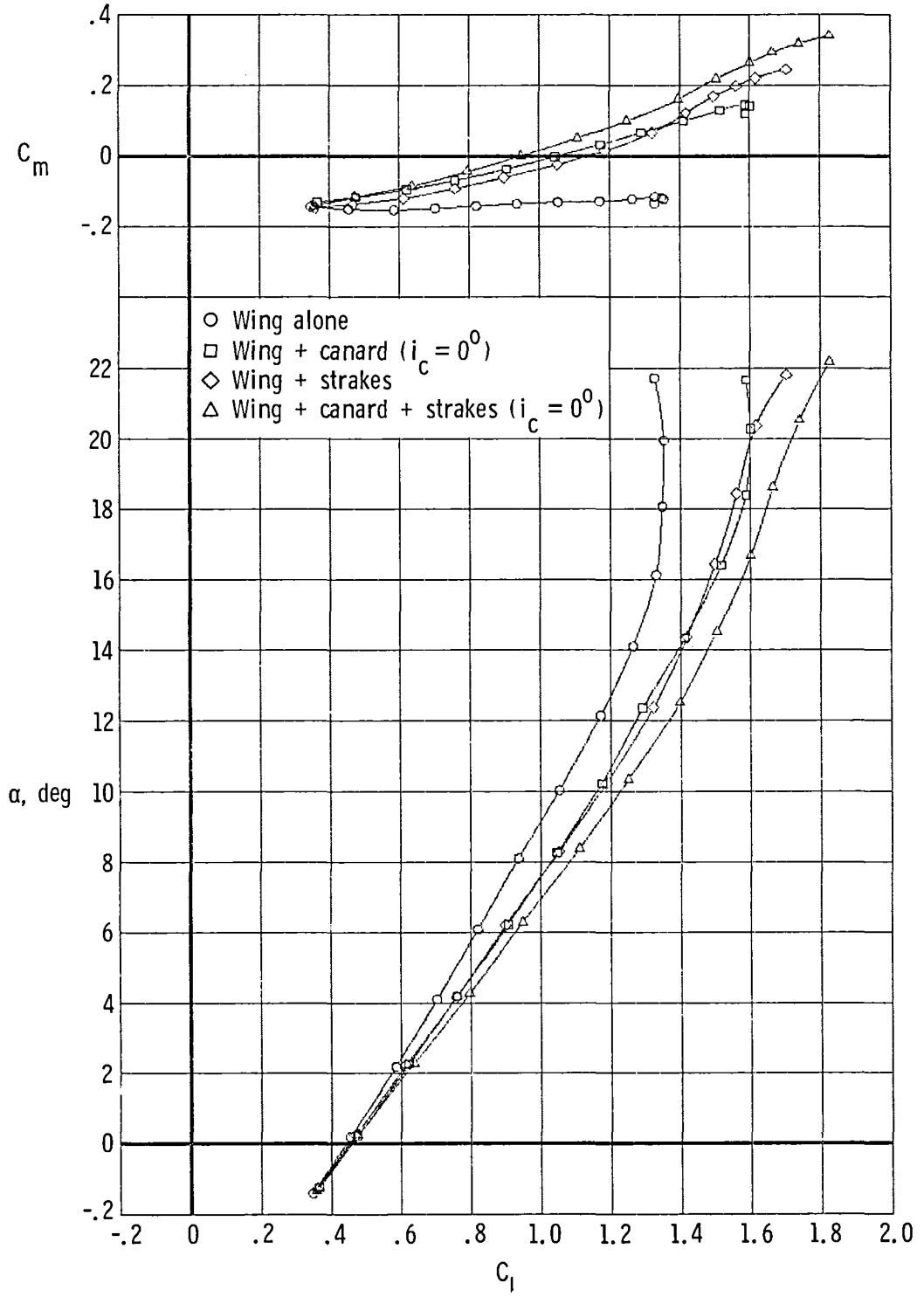

(a) Lift and pitching moment.

Figure 9.- Comparison of different wing, canard, and strake combinations. $\delta_{le} = 10°$; $\delta_{te} = 10°$.

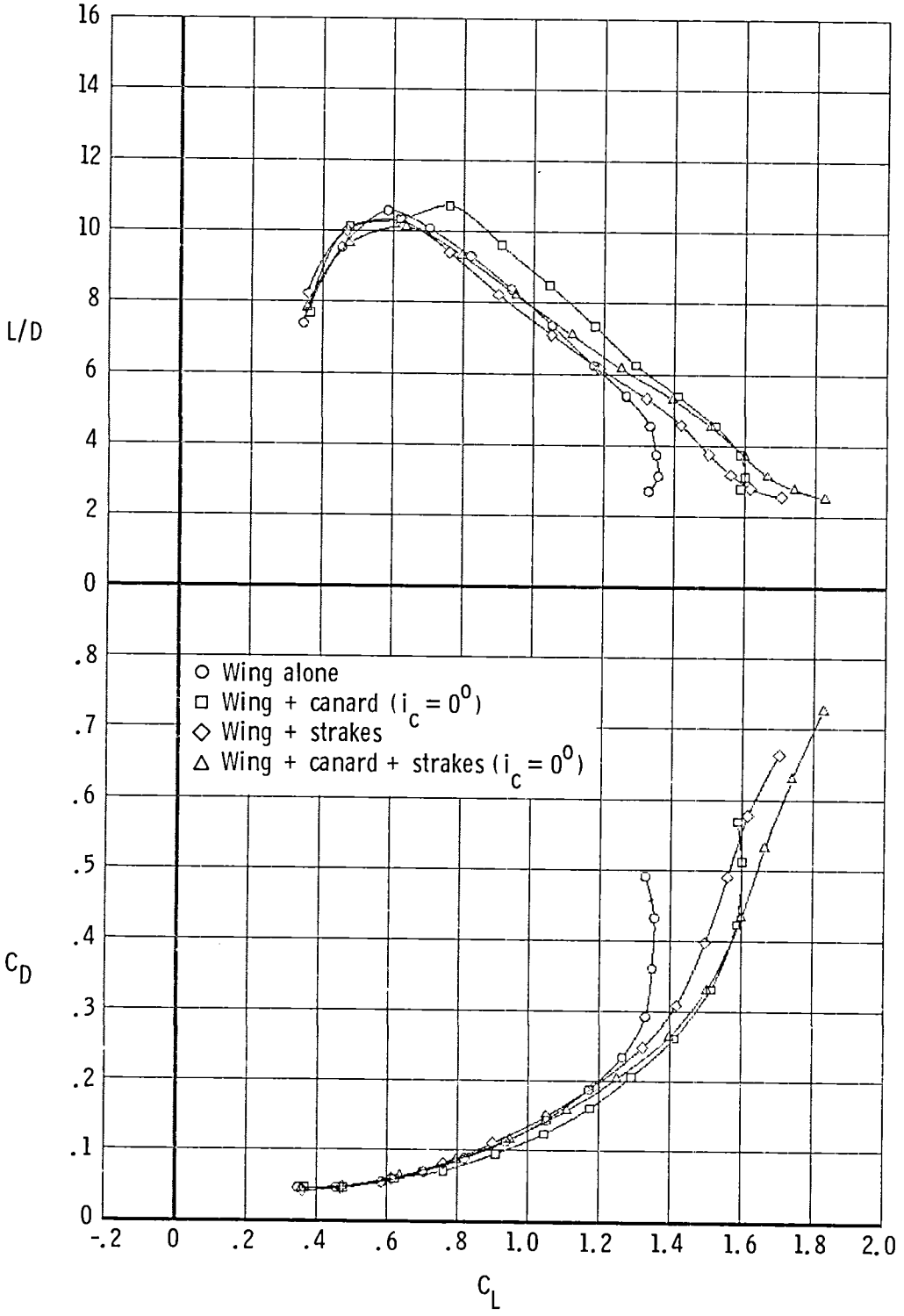

(b) Drag and L/D.

Figure 9.- Concluded.

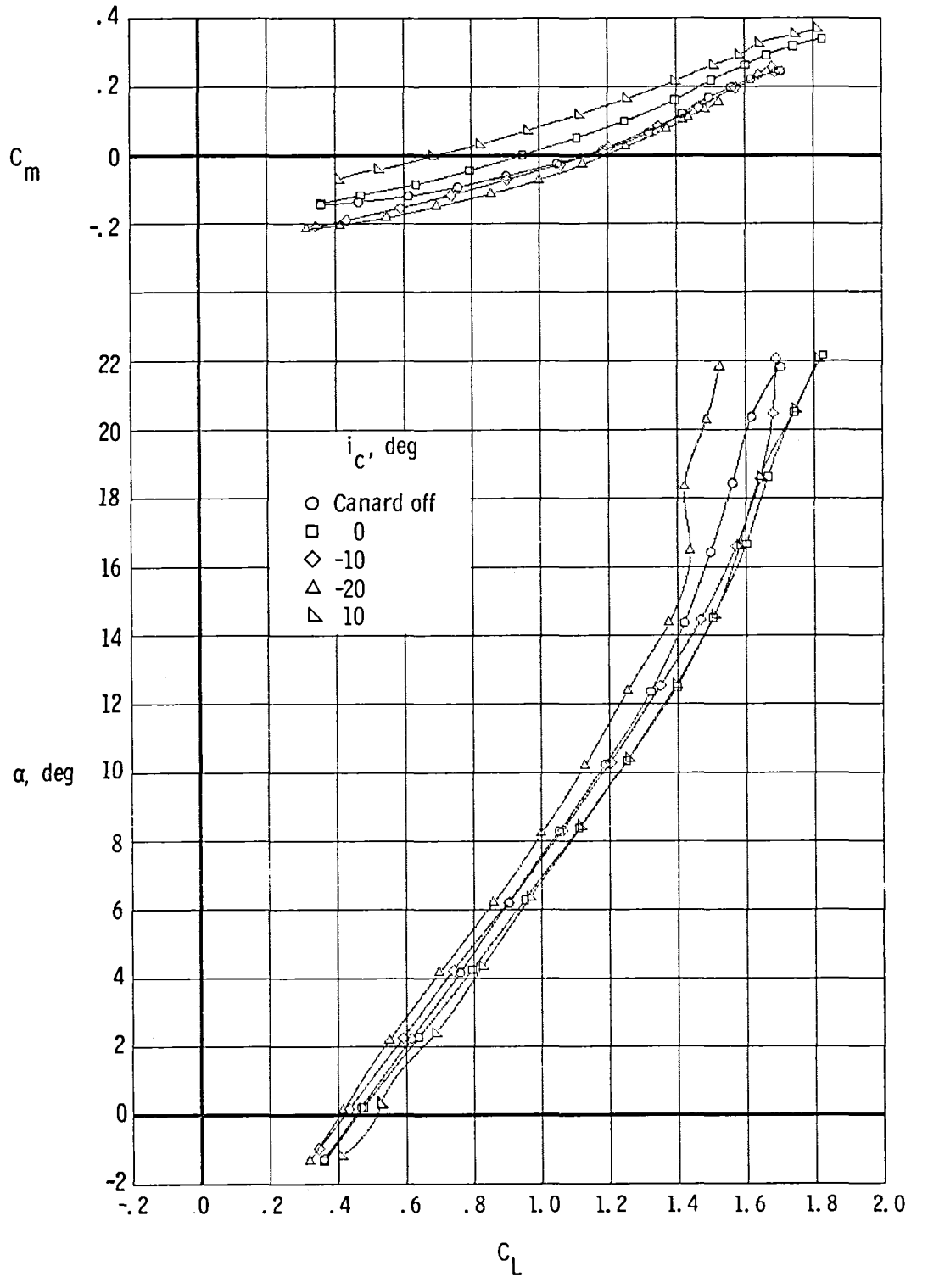

(a) Lift and pitching moment.

Figure 10.- Effects of canard incidence for wing-plus-canard-plus-strakes configuration. $\delta_{le} = 10°$; $\delta_{te} = 10°$.

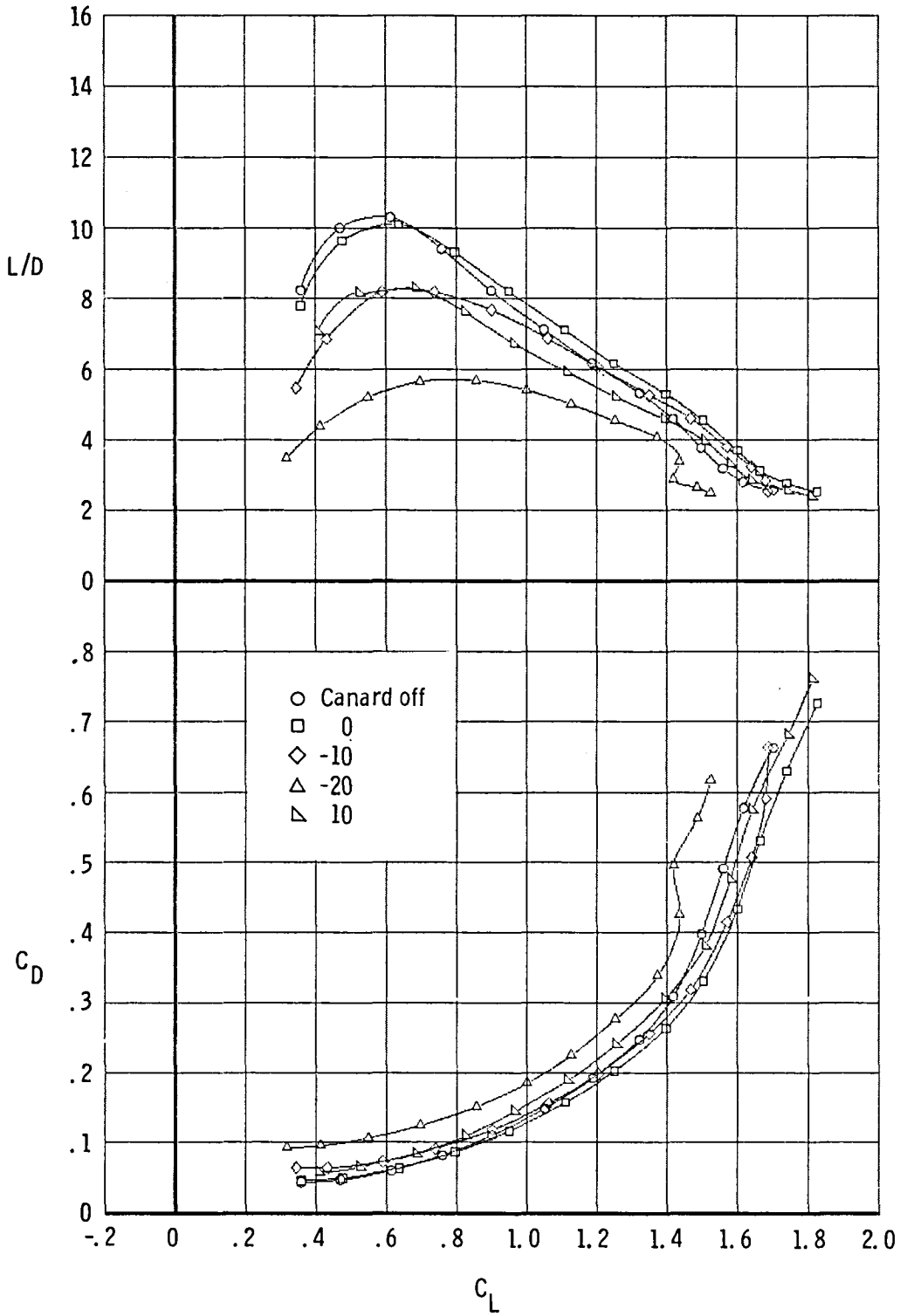

(b) Drag and L/D.

Figure 10.- Concluded.

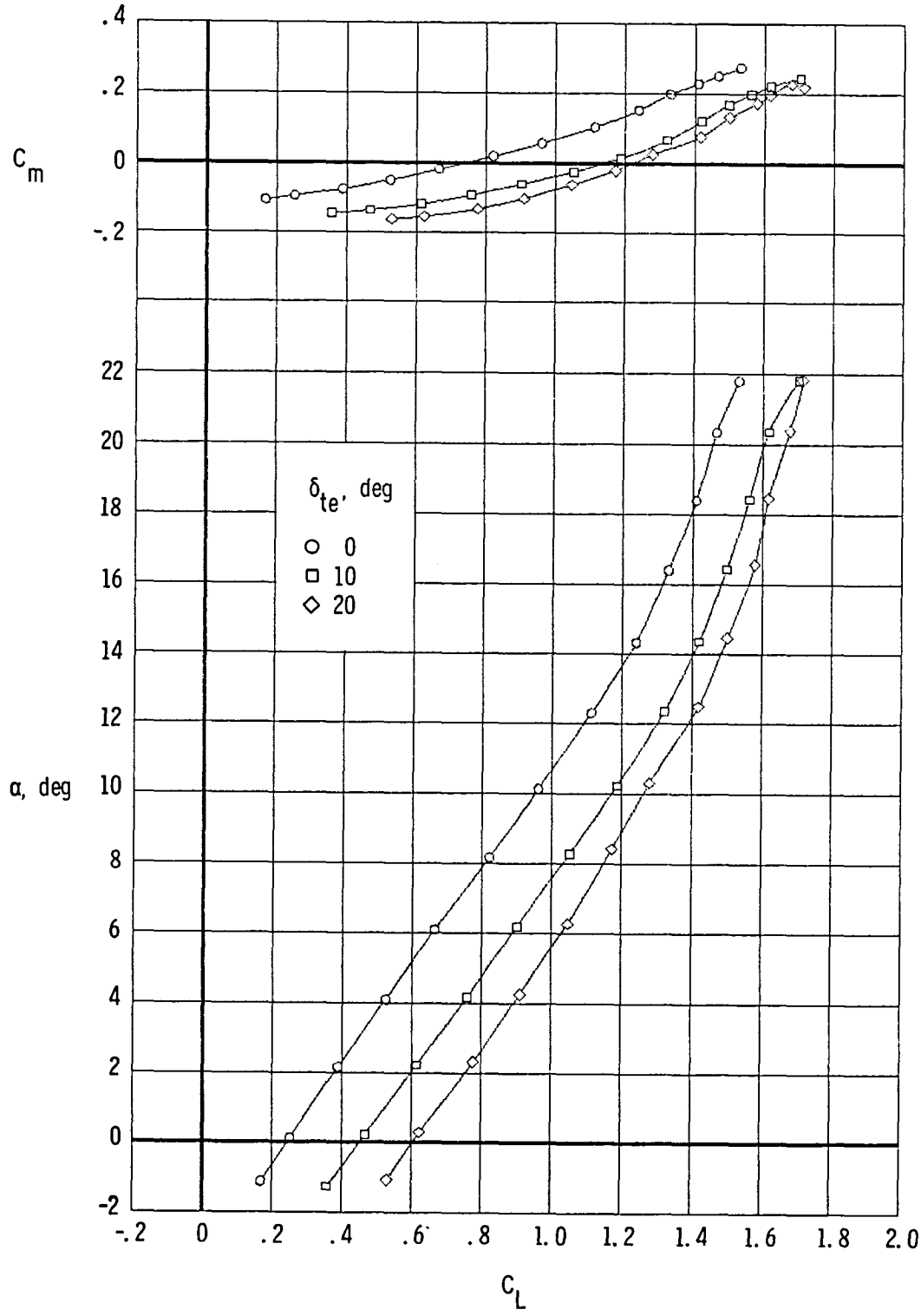

(a) Lift and pitching moment.

Figure 11.- Effects of trailing-edge flap deflection for wing-plus-strakes configuration. δ_{le} = 10°.

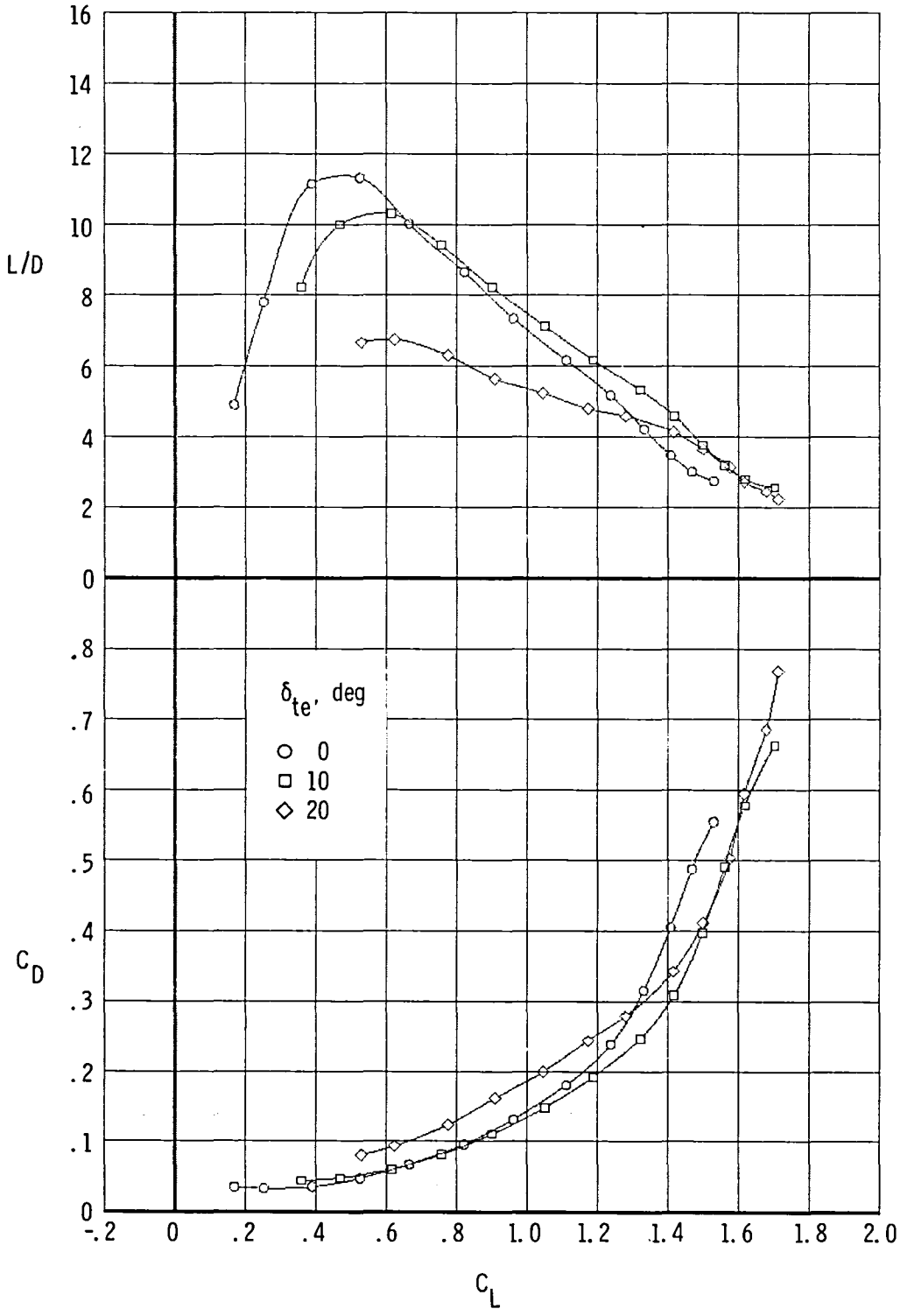

(b) Drag and L/D.

Figure 11.- Concluded.

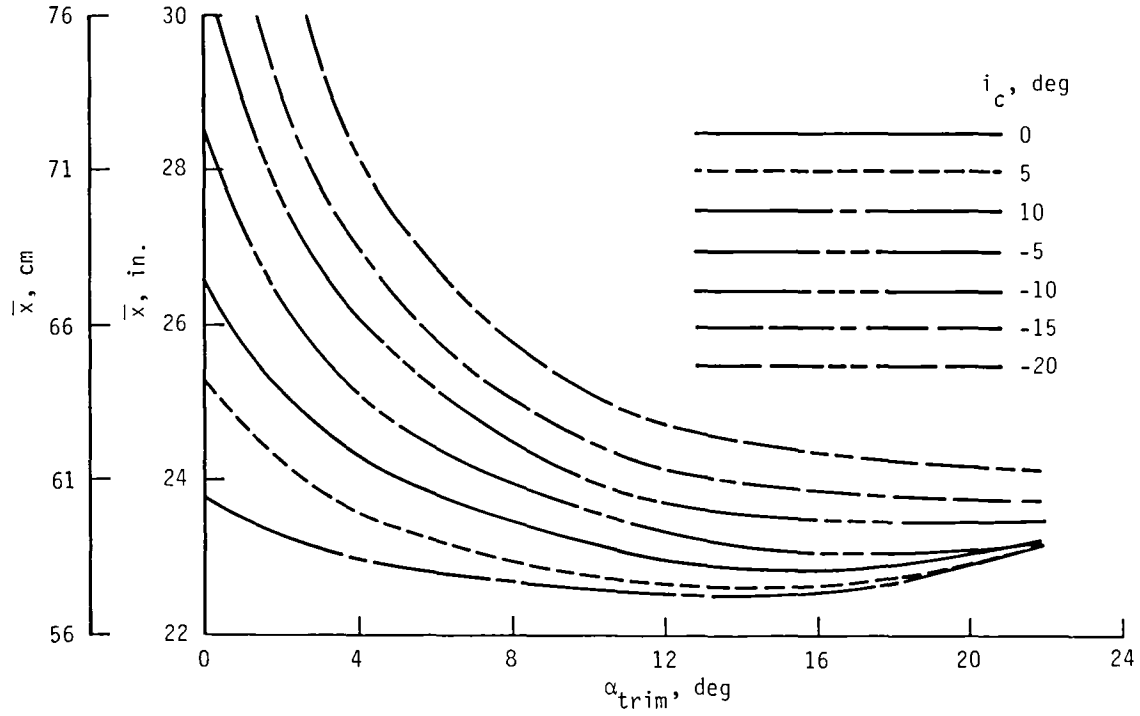

(a) $\delta_{le} = 0°$; $\delta_{te} = 0°$.

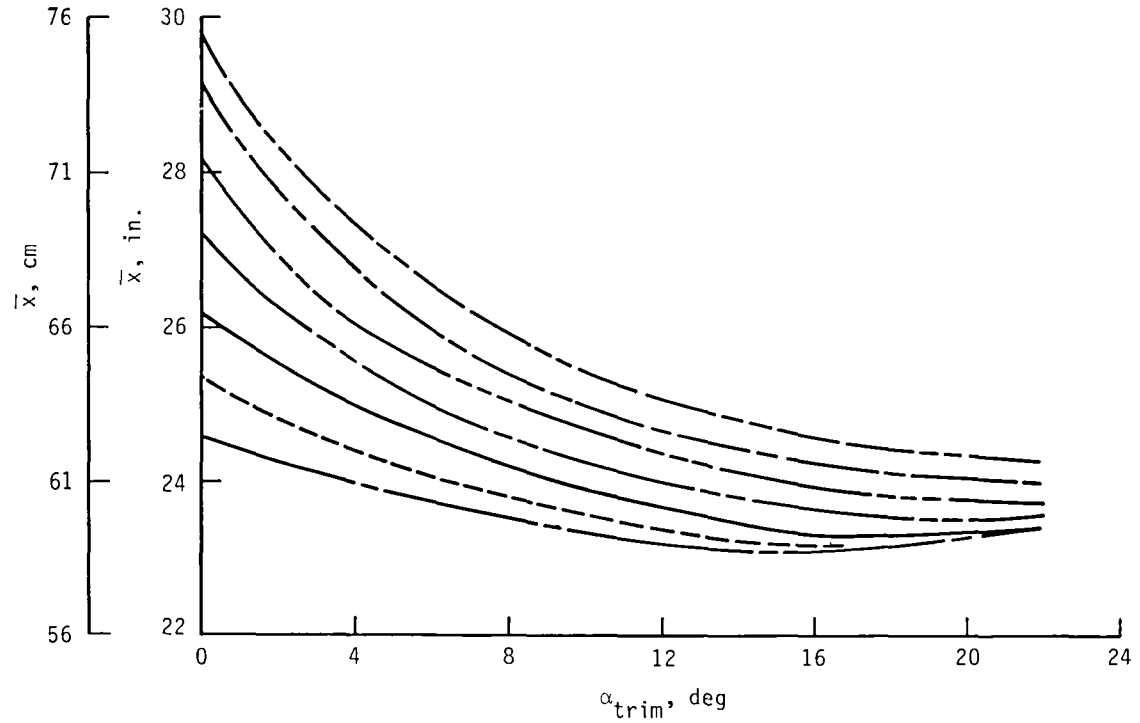

(b) $\delta_{le} = 10°$; $\delta_{te} = 20°$.

Figure 12.- Moment reference center locations required for trim.

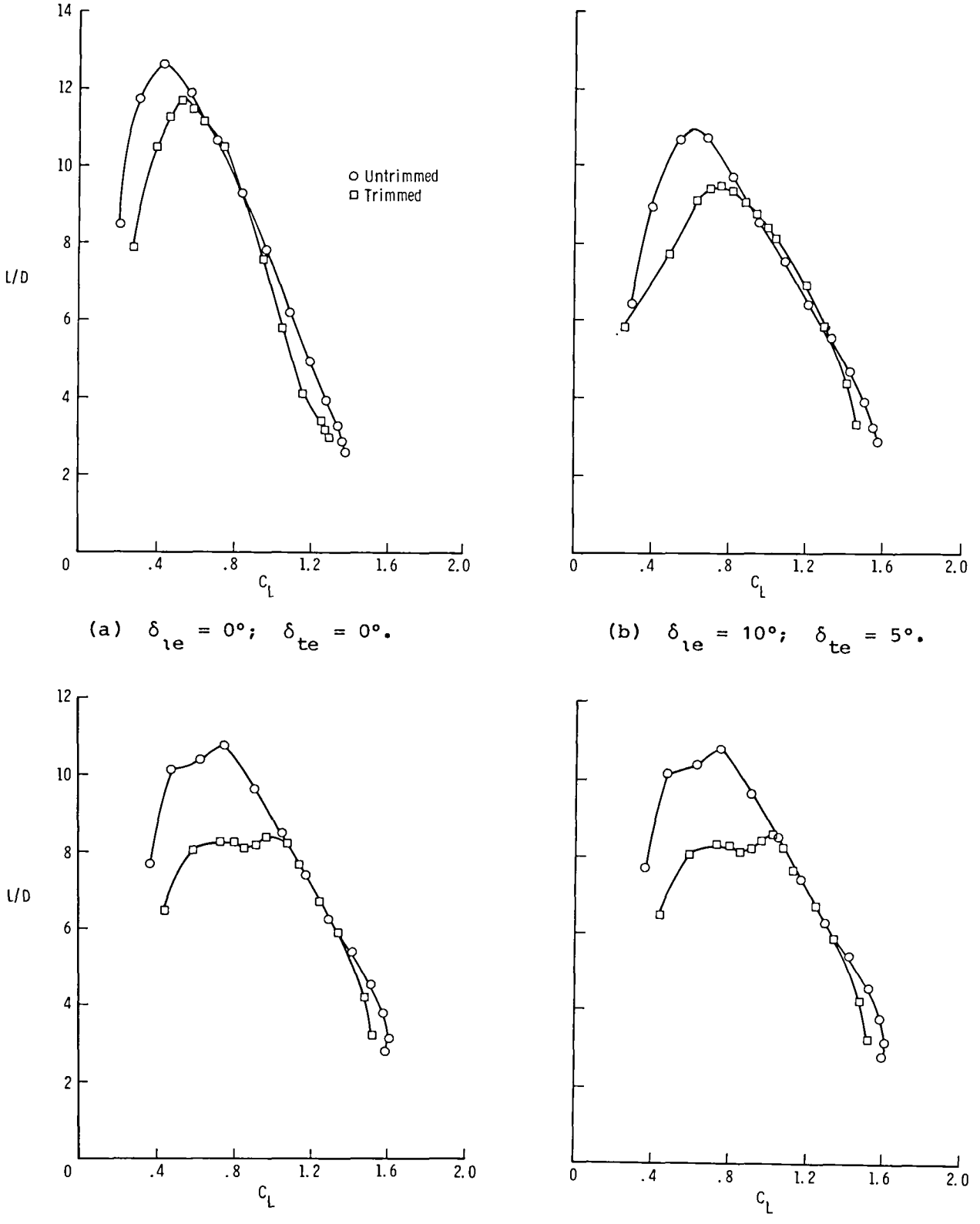

(a) $\delta_{le} = 0°$; $\delta_{te} = 0°$.

(b) $\delta_{le} = 10°$; $\delta_{te} = 5°$.

(c) $\delta_{le} = 10°$; $\delta_{te} = 10°$.

(d) $\delta_{le} = 10°$; $\delta_{te} = 20°$.

Figure 13.- Comparison of trimmed and untrimmed lift-drag ratios.

1. Report No.	2. Government Accession No.	3. Recipient's Catalog No.
NASA TM-85795		

4. Title and Subtitle	5. Report Date
LOW-SPEED INVESTIGATION OF EFFECTS OF WING LEADING- AND TRAILING-EDGE FLAP DEFLECTIONS AND CANARD INCIDENCE ON A FIGHTER CONFIGURATION EQUIPPED WITH A FORWARD-SWEPT WING	July 1984
	6. Performing Organization Code: 505-43-23-06

7. Author(s)	8. Performing Organization Report No.
Thomas G. Gainer, Michael J. Mann, and Jarrett K. Huffman	L-15746
	10. Work Unit No.

9. Performing Organization Name and Address	11. Contract or Grant No.
NASA Langley Research Center Hampton, VA 23665	
	13. Type of Report and Period Covered: Technical Memorandum

12. Sponsoring Agency Name and Address	14. Sponsoring Agency Code
National Aeronautics and Space Administration Washington, DC 20546	

15. Supplementary Notes

An electronic data tape is available as a supplement to this report.

16. Abstract

An advanced fighter configuration with a forward-swept wing of aspect ratio 3.28 was tested in the Langley 7- by 10-Foot High-Speed Tunnel at a Mach number of 0.3. The wing had 29.5° of forward sweep of the quarter-chord line and was equipped with 15-percent-chord leading-edge and 30-percent-chord trailing-edge flaps. The canard was sweptback 45°. Tests were made through a range of angle of attack from about -2° to 22°. The test results showed that deflecting the flaps significantly improved the lift-drag characteristics at the higher angles of attack. The canard was able to trim the configurations with different flap deflections over most of the range of angle of attack. The penalty in maximum lift coefficient due to trimming was about 0.10.

17. Key Words (Suggested by Author(s))	18. Distribution Statement
Forward sweep Fighters Flaps Canards	Unclassified - Unlimited Subject Category 02

19. Security Classif. (of this report)	20. Security Classif. (of this page)	21. No. of Pages	22. Price
Unclassified	Unclassified	49	A03

For sale by the National Technical Information Service, Springfield, Virginia 22161 NASA-Langley, 1984